

General Disclaimer

One or more of the Following Statements may affect this Document

- This document has been reproduced from the best copy furnished by the organizational source. It is being released in the interest of making available as much information as possible.
- This document may contain data, which exceeds the sheet parameters. It was furnished in this condition by the organizational source and is the best copy available.
- This document may contain tone-on-tone or color graphs, charts and/or pictures, which have been reproduced in black and white.
- This document is paginated as submitted by the original source.
- Portions of this document are not fully legible due to the historical nature of some of the material. However, it is the best reproduction available from the original submission.

NASA Grant NGL 39-009-015(8)



THE PENNSYLVANIA
STATE UNIVERSITY



Scientific Report No. 017

A 36 GHz TRAVELING WAVE ^{MASER} ~~MASTER~~ FOR USE
IN RADIO ASTRONOMY

by

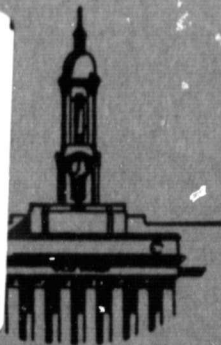
Paul N. Swanson

January 27, 1969

RADIO ASTRONOMY OBSERVATORY

DEPARTMENT OF ASTRONOMY

N 69-22814	(ACCESSION NUMBER)	(THRU)	
94	(PAGES)	1	(CODE)
	(NASA CR OR TMX OR AD NUMBER)	16	(CATEGORY)



The Pennsylvania State University
College of Science

Radio Astronomy Observatory
NASA Grant NGL 39-009-015(8)

Scientific Report

on

"A 36 GHz Traveling Wave Maser for Use
in Radio Astronomy"

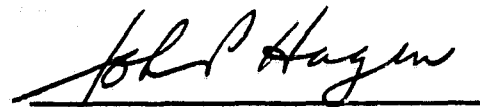
by

Paul N. Swanson

January 27, 1969

Scientific Report No. 017

Approved by:


John P. Hagen, Head
Department of Astronomy

The Pennsylvania State University

College of Science

Department of Astronomy

TABLE OF CONTENTS

	Page
LIST OF TABLES	iv
LIST OF FIGURES	v
I. INTRODUCTION	1
A. Need for Millimeter Wave Maser Amplifier	1
Receiver noise	1
Receiver sensitivity	3
Low noise receivers	4
B. Outline of Research Program	5
II. THE MASER--Theory of Operation	6
Elementary considerations	6
Paramagnetic energy levels	12
Quantum mechanical calculations; the perturbation Hamiltonian	15
Einstein A & B coefficients and radiation	29
The three level maser	32
The traveling wave maser	35
III. THE 36 GHz TRAVELING WAVE MASER	37
A. Design Requirements for Intended Use in Radio Astronomy	37
B. Specific Maser Design	39
Active material	39
Crystal orientation and energy levels	41
Slow wave structure	42
C. Experimental Apparatus	47
Description of cryogenic system	47
Description of superconducting magnet	47
Description of microwave hardware	49
D. Construction and Testing of Maser	52
Rutile crystals	52
Reduced size waveguide	53
Tapered transitions	54
Rutile dielectric constant	55
Measurement of dielectric constant	59
Prototype maser	65
Operation with larger cross section crystals	69
Ferrite isolator	71

TABLE OF CONTENTS (Continued)

	Page
E. Final Maser Amplifier	75
Description	75
Maser operation	75
Gain and bandwidth	78
Comparison with theory	79
IV. SUMMARY	81
A. Statement of Problem	81
B. Procedure	81
C. Results	81
D. Suggestions for Future Work	82
APPENDIX I. Secular Equation Computer Program	84
APPENDIX II. Rutile Crystal Structure	86
BIBLIOGRAPHY	88

LIST OF TABLES

Table	Page
1. Dielectric Constant of Rutile	68
2. Maser Operating Parameters	77

LIST OF FIGURES

Figure	Page
1. Schematic Maser Radiometer	7
2. Spin Paramagnetic Resonance	9
3. Population Distribution	11
4. Spin Hamiltonian Coordinate System for Rutile	24
5. Push-Pull Energy Levels in Rutile	28
6. 36 GHz Slow Wave Structure	46
7. Experimental Apparatus for Maser Testing	48
8. Superconducting Magnet System	50
9. Tapered Transition	56
10. Attenuation in Partially Filled Waveguide	58
11. Method of Measuring Dielectric Constant	62
12. ϵ and δ for Rutile at 300°K	64
13. Prototype Maser	66
14. 36 GHz Maser	76
15. Crystal Structure of Rutile and the Magnetic Axes	87

I. INTRODUCTION

A. Need for Millimeter Wave Maser Amplifier

Receiver noise

A radio frequency (r.f.) receiver accepts radiation from the terminals of an antenna and amplifies this radiation to a level where it can easily be detected and presented in an audio or visual fashion. Intrinsic in this process is the addition of unwanted broadband radiation (radio noise) originating in the receiver itself.

In radio astronomy, the observed radio signals, with few exceptions, consist entirely of noise. This observed noise cannot readily be differentiated from the noise generated in the receiving system itself.

The amount of receiver noise internally generated can be measured quantitatively and is indicated by the receiver noise figure or noise factor. However, before the noise figure is defined it is necessary to define noise temperature, T .

If an electrical resistance is placed in an oven at temperature T , then the total available noise power P , measured across the terminals of the resistor will be given by

$$P = kTB \quad (1)$$

where

k = Boltzmann's constant

B = frequency bandwidth of the measurement.

This is the well known Nyquist or Johnson noise theorem. Equation (1) can be generalized so that the noise power output, P_n , of any device defines an effective noise temperature T_e , where

$$P_n \equiv k T_e B. \quad (2)$$

If the input terminals of a receiver are terminated in a matched impedance at a temperature T_o , then the noise power available at the output of the receiver is defined to be ⁽¹⁾

$$P_n \equiv F G k T_o B, \quad (3)$$

where

G is the gain of the receiver and

F is the noise factor of the receiver.

The portion of this power due to the noise arising at the input termination from equation (1) is $G k T_o B$. Thus, the noise power originating in the receiver itself is

$$P_r = (F - 1) G k T_o B . \quad (4)$$

This is actually the defining equation for the noise factor F . In equation (4), T_o usually is taken to be 290°K . F is then a measure of the amount of noise contributed by the receiver. Two commonly used terms related to F are:

$$\text{receiver noise figure} \quad F(\text{db}) \equiv 10 \log_{10} F \quad (5)$$

$$\text{receiver effective noise temperature} \quad T_r = (F - 1) T_o . \quad (6)$$

T_r is used more often when referring to low noise receivers with ($T_r < 300^\circ\text{K}$)

Receiver sensitivity

The noise figure $F(\text{db})$ is not a direct measure of the usefulness of a receiver in any particular application. A better criterion is that of minimum detectable temperature ΔT_{min} . It can be shown from information theory that (2)

$$\Delta T_{\text{min}} = \frac{T_{\text{ant}} + (F - 1) T_o}{\sqrt{B\tau}} , \quad (6)$$

where T_{ant} is the effective antenna temperature of the observed radio source, τ is the output integration time of the receiver, and F and B are the noise factor and bandwidth as defined previously. It can be seen that a low noise receiver ($(F - 1) T_o \approx 100^\circ\text{K}$) is not necessary in a solar observation where the antenna temperature may exceed $6,000^\circ\text{K}$, for example. On the other hand, a weak radio source may have $T_{\text{ant}} \approx 1^\circ\text{K}$ where it is desirable to minimize F .

T_{ant} may include radiation other than that from the source. Side and back lobes may pick up ground radiation, and at both very high and low frequencies the earth's atmosphere becomes lossy. The low frequency attenuation is due to the ionosphere. The microwave attenuation is due to rotational and vibrational spectra of oxygen and water vapor. A lossy atmosphere not only attenuates the source signal but also reradiates thermal noise. An additional source of low frequency radiation is the galactic background. Fortunately, there are "atmospheric windows" in the millimeter region of the radio spectrum. The 36 GHz atmospheric window can have as little as 0.5 db loss and thus contribute less than 30°K to antenna temperature.

Low noise receivers

The most common type of radio frequency receiver is the superheterodyne with crystal mixing. The point contact diodes used for mixing are the major noise contributor in these receivers when used at microwave or higher frequencies. The noise is generated primarily by the shot effect from the unavoidable d.c. current through the crystal.

Another type of low noise microwave receiver uses a parametric amplifier where the mixing is done in a variable capacitor or inductor. This mixer, as opposed to crystal mixing, produces a net gain; furthermore it has no resistive component

to produce Johnson noise. The inherent low noise properties of parametric amplifiers are partially offset by the fact that being single port devices they require a circulator in the input. The circulator has a resistive component which attenuates the input signal and introduces noise.

A maser amplifier does not depend on mixing at all. In a maser, the signal gains energy by stimulated emission in some paramagnetic ion. Since a maser usually operates at liquid helium temperatures, any resistance in the amplifier can contribute a maximum of 4.2°K to receiver noise. The first masers were single port, cavity type which required a circulator, as with a parametric amplifier. However, the traveling wave maser is a two port device, requires no circulator and is completely cooled to liquid helium temperatures. The only noise contribution above 4.2°K comes from the antenna and input waveguide which are present in any system.

B. Outline of Research Program

The object of this research project was to develop a low noise traveling wave maser radiometer for use in radio astronomy at a frequency of 36 GHz.

The first step of the program was to make a theoretical analysis of a 36 GHz traveling wave maser, making use of data from other maser amplifiers and electron paramagnetic resonance (EPR)

experiments. This analysis was undertaken to produce an optimum design, considering intended use, paramagnetic materials available, energy levels, magnetic field and practical problems of construction.

The second part of the program was the construction of a prototype maser for the determination of energy levels, gain per unit length of slow wave structure, bandwidth nonreciprocity, etc. Operation (or nonoperation) of the prototype would indicate deviations from the theoretical analysis which could then be corrected in the final maser amplifier.

Other millimeter maser projects are listed in the references. (11,12,13,14,15,16)

II. THE MASER--Theory of Operation

Elementary consideration

In a traveling wave maser radiometer (Figure 1) the r.f. signal power travels from the antenna down some type of transmission line to the slow wave structure where the signal interacts with a group of paramagnetic ions, gains energy at the expense of pump power, and emerges on the output transmission line. The amplified signal is then processed in a conventional manner; i.e., by going into a superheterodyne receiver.

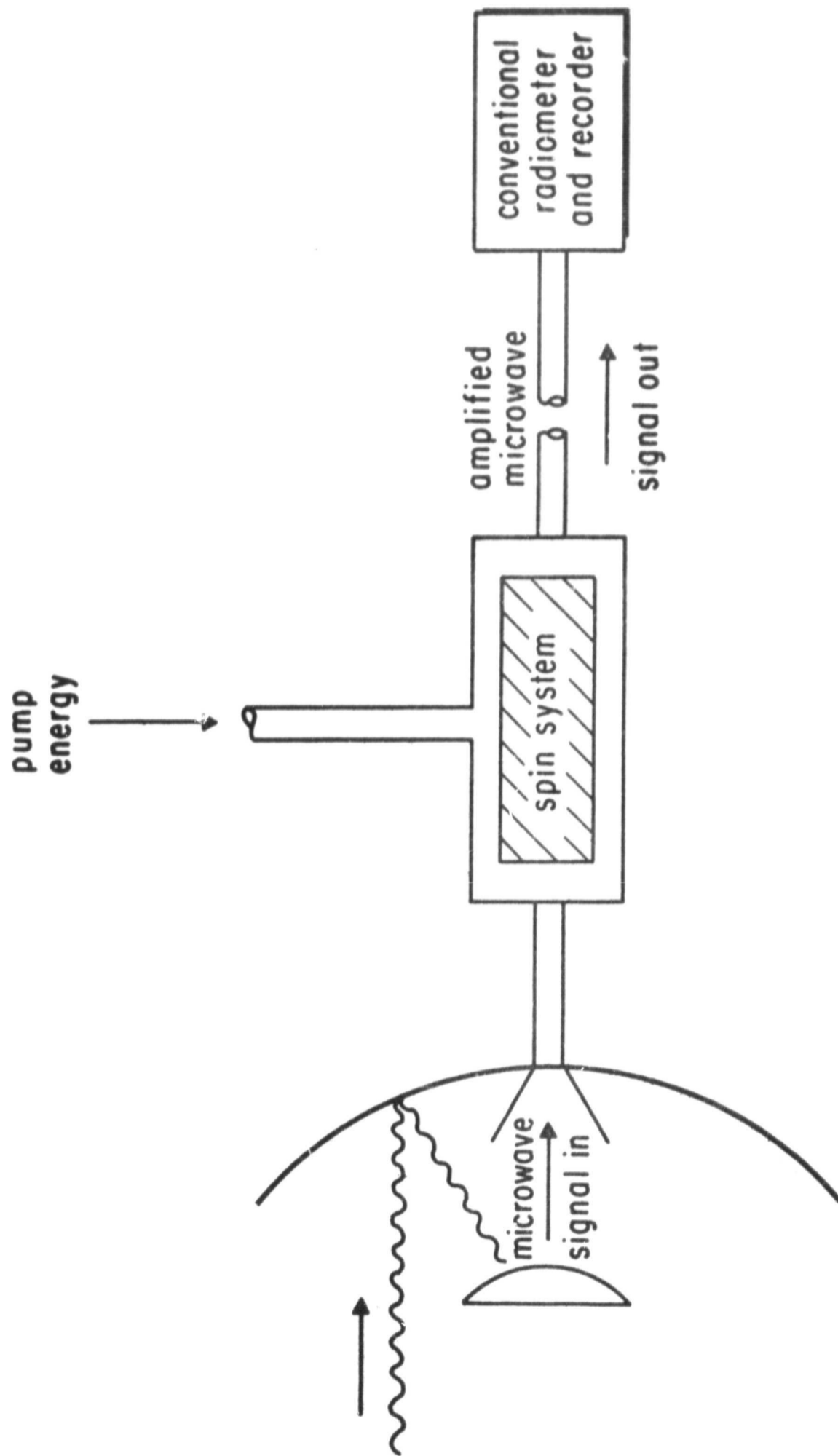


Figure 1 - Schematic Maser Radiometer

The manner in which the r.f. signal and pump power interact with the paramagnetic ions to amplify the signal is the crucial point in understanding maser operation.

Paramagnetic resonance is based on the fact that when an ion possessing a resultant angular momentum (from one or more unpaired electrons) is placed in a d.c. magnetic field, the angular momentum vector will precess about the axis of the d.c. magnetic field, H , with a frequency $\nu = \gamma H$ where $\gamma = 2.8$ MHz/gauss for electrons (Figure 2a). If the ion is in its lowest energy state, a circularly polarized magnetic field (the r.f. signal or pump) with frequency ν and the correct sense of polarization will cause the ion to jump to the next higher energy level while absorbing a photon of energy from the r.f. field. The energy absorbed is given by the Planck relation $E = h\nu$ where $h =$ Planck's constant. If the ion is in one of its higher energy states originally, the r.f. field can cause the ion to emit a photon of energy, $E = h\nu$ (stimulated emission). Figure 2b is an energy level diagram for an electron (or an ion with one unpaired electron). The electron can exist in only two states, "spin-up" or "spin-down". The frequency of the photon emitted or absorbed during a transition is determined by the value of H and is equal to $\nu = \gamma H$. The energy of the transition is

$$E = h\nu = h \gamma H . \quad (7)$$

In a two electron system, three energy states $S = 1$ (both spins down), $S = 0$ (one up, one down), and $S = -1$ (both spins up) are possible (see Figure 2c). If we take a large number of ions,

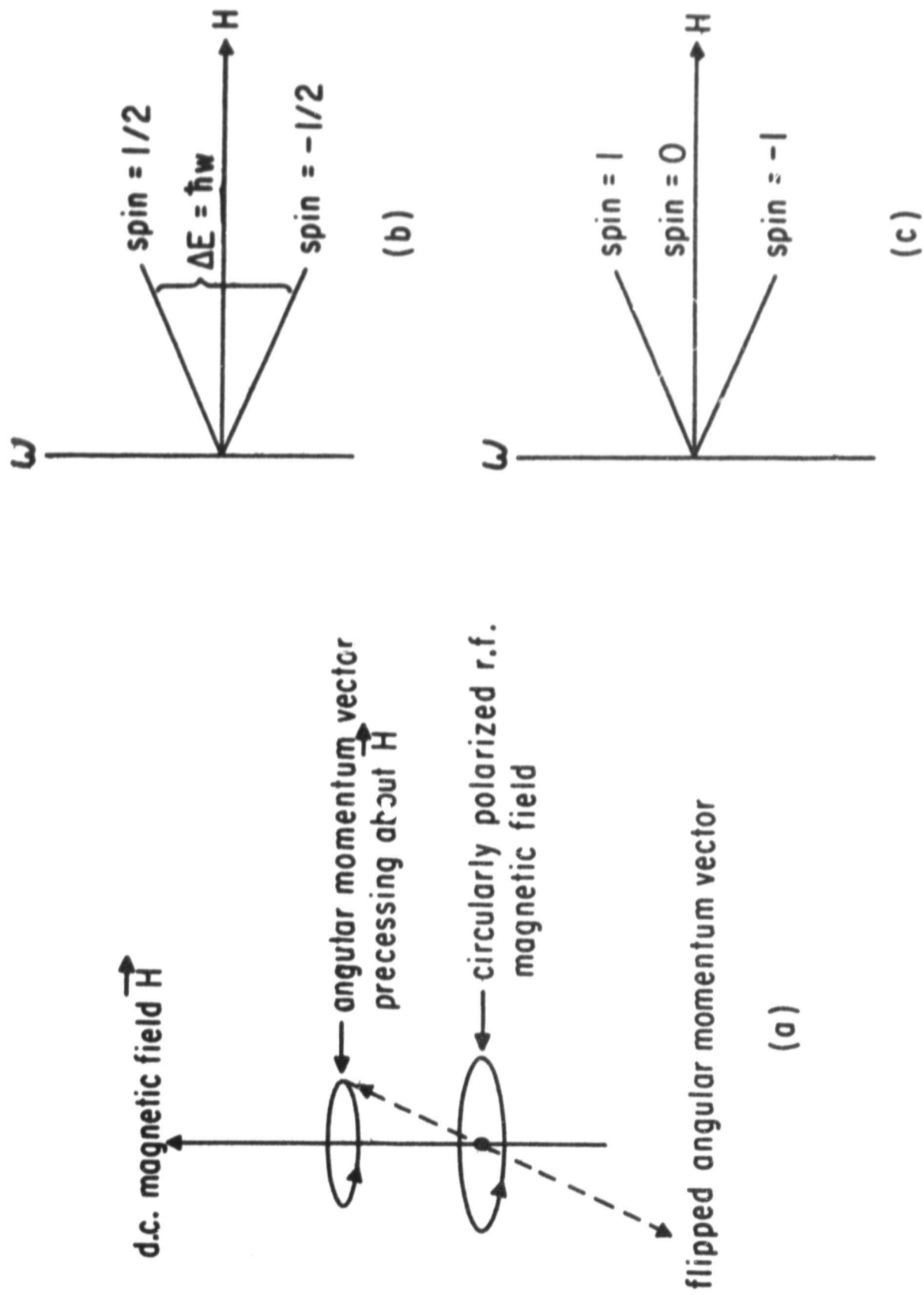


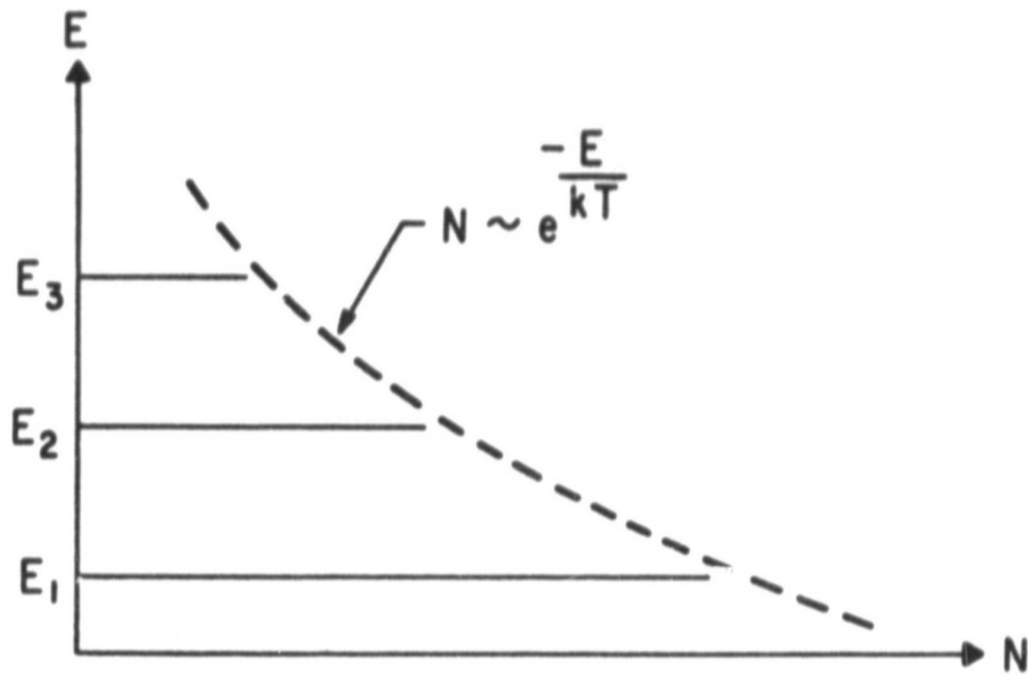
Figure 2 – Spin Paramagnetic Resonance

each with two unpaired electrons, and look at the number of ions in each of the three energy states when in thermal equilibrium, we find that most of the ions are in the lowest energy level. In fact, the population of the energy levels is a Boltzmann distribution given by

$$\frac{N_i}{N_j} = \frac{g_i}{g_j} \exp \left(\frac{E_j - E_i}{kT} \right) \quad (8)$$

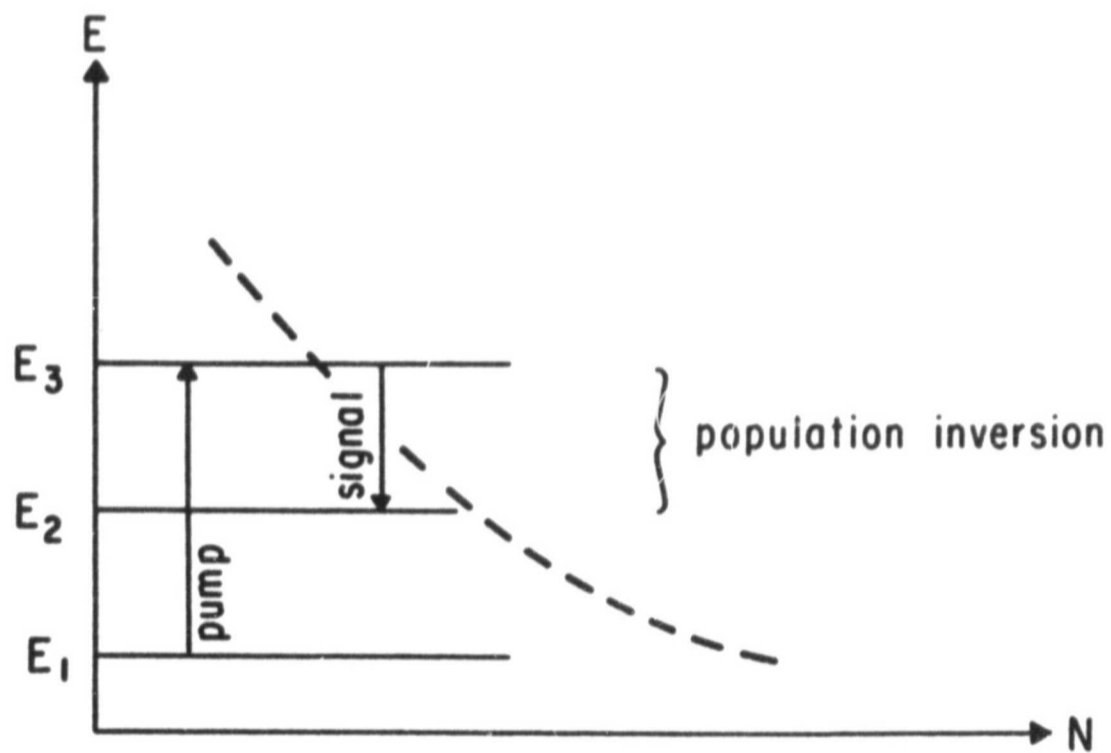
where N_i is the population of the i^{th} energy level E_i , g_i is the statistical weight of the i^{th} level, k is the Boltzmann constant and T is the absolute temperature (Figure 3a). In the nondegenerate case of Zeeman energy levels, the g_i are unity. If r.f. pump energy with frequency $\nu = \frac{E_3 - E_1}{h}$ and the proper circular polarization contacts the spin system, there will be stimulated upward transitions from level 1 to level 3. The population will be changed to that shown in Figure 3b with N_3 increased and N_1 decreased. There is now a population inversion (as compared to the equilibrium distribution) of levels 3 and 2. This inversion will be maintained as long as a strong pump signal persists. Now a weak signal of $\nu = \frac{E_3 - E_2}{h}$ contacting the system will stimulate downward transitions from level 3 to level 2. These emitted photons will add to the input signal coherently and thus amplify the input signal.

We will now supplement this heuristic approach with a more rigorous treatment of maser operation using quantum mechanical calculations where necessary. First, we will consider the energy levels and the interaction of the magnetic field with the total angular momentum of an ion along with such perturbations as crystalline field effects; then we will consider the rate equations which determine the



(a)

Equilibrium population distribution



(b)

Inverted population distribution

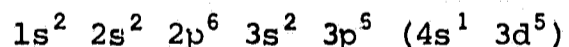
Figure 3 - Population Distributions

population of the energy levels when in equilibrium with radiation fields. Finally, the general equations governing a 3-level maser will be developed.

Paramagnetic energy levels

The ions useful for solid state masers belong to one of the transition group elements, usually the iron transition group. In these groups the most commonly used are Cr and Fe. The transition group elements are characterized by partially filled inner electron shells. In chemical binding only the outer or valence electrons enter into the bonds and these electrons in most cases are magnetically neutralized by forming pairs with the valence electrons of the other element. In the case of chemical binding with the transition group elements the inner, unfilled shell has unpaired electrons which give rise to a net magnetic moment.

Since we will be concerned here with chromium ($Z = 24$), consider its electronic configuration of



where the standard notation of $n\ell^m$ is used. In this notation n is the principal quantum number, ℓ is the orbital angular momentum and m is the number of electrons in the $n\ell$ electron shell. The parenthesis indicates the transition group where the 4s shell fills before the 3d shell. Spectroscopic notation is used for the orbital angular momentum where s implies $\ell = 0$, p implies $\ell = 1$, d implies $\ell = 2$, and f implies

$l = 3$. In the actual maser, chromium is introduced as an impurity into a host lattice of TiO_2 (rutile). It is then in the +3 ionization state due to its chemical bonding with the TiO_2 . This leaves 3 unpaired 3d electrons in the Cr^{+3} ion. Each electron can have a spin of $\pm 1/2$ and a z-component of orbital angular momentum m_l of 2, 1, 0, -1 or -2. Considering first a free Cr^{+3} ion, the Pauli exclusion principle states that no two electrons can have identical quantum numbers. Using this and a semiempirical set of rules, called Hund's rules, we can now find the ground state of the Cr^{+3} ion. Hund's rules state that the electrons will be distributed inside a given shell in such a way as to (1) maximize the magnitude of the sum of m_s over all the electrons in the shell and (2) then maximize the magnitude of the sum of m_l over all the electrons in the shell, consistent with the Pauli principle. Rule (1) demands that all three electron spins be aligned, giving $S = 1/2 + 1/2 + 1/2 = 3/2$. The second rule requires that the first electron have a $m_l = 2$, the second $m_l = 1$ and the third $m_l = 0$ giving $L = 2 + 1 + 0 = 3$. In the Russell Saunders or L-S coupling scheme the total spin and orbital angular momentum couple together to give a resultant vector called J , i.e. $\vec{L} + \vec{S} = \vec{J}$. J can take on the values $L-S, L-S+1, \dots, L+S$. According to a third Hund rule the ground state J for a less than half filled shell is $L-S$ or $3 - 3/2 = 3/2$ for Cr^{+3} . This can all be written in spectroscopic notation

$${}^{2S+1}L_J$$

which gives for the chromium ion ground state a ${}^4F_{3/2}$ state.

The orientation energy of a magnetic dipole, $\vec{\mu}$, in a magnetic field is

$$E = -\vec{\mu} \cdot \vec{H} . \quad (9)$$

The magnetic dipole moment of an orbiting electron is

$$\vec{\mu}_e = -\beta \vec{L}$$

and for electron spin

$$\vec{\mu}_s = -2\beta \vec{S}$$

where β is called the Bohr magneton;

$$\beta = \left(\frac{e\hbar}{2mc} \right) = 9.27 \times 10^{-21} \text{ erg/gauss} .$$

The magnetic moment for the total angular momentum, \vec{J} , can be written as

$$\vec{\mu}_J = -g_J \beta \vec{J} , \quad (10)$$

where g_J is called the Landé g factor and has the value one for orbital angular momentum and two for spins. For a free atom or ion following the Russel-Saunders spin-orbit coupling scheme when both L and S are present, it can be shown by a strict quantum mechanical calculation⁽¹⁷⁾ that

$$g_J = 1 + \frac{J(J+1) + S(S+1) - L(L+1)}{2J(J+1)} . \quad (11)$$

Combining (9) and (10),

$$E = g_J \beta \vec{J} \cdot \vec{H} .$$

If we take \vec{H} to be in the z -direction then the product $\vec{J} \cdot \vec{H}$ is the projection of \vec{J} on the z -axis and is just the quantum number M_J multiplied by H . The preceding equation then becomes

$$E = g_J \beta M_J H . \quad (12)$$

Equation (12) gives the energy levels for the familiar Zeeman effect. An atom or ion with a total angular momentum J will be $2J+1$ -fold space degenerate. The application of a magnetic field, H , will remove this degeneracy and split the various J multiplets into $2J+1$ Zeeman levels. The levels are labeled M_J and have the values $J, J-1, \dots, -J$.

The Cr^{+3} Zeeman levels can easily be found using the ${}^4F_{3/2}$ ground state previously determined. The value of J for the ground state is $3/2$ which gives $2(3/2) + 1 = 4$ Zeeman levels, labeled $M_{3/2}, M_{1/2}, M_{-1/2}, M_{-3/2}$. g_J can be calculated from equation (11) and the energies from equation (12).

The previous discussion applies to a free atom or ion. We will now consider the practical situation of the ion in a crystal lattice as an impurity ion. Although the ground state is still the ${}^4F_{3/2}$ state, there are important differences from the isolated case due to the strong interaction with the crystalline electric fields. In this case, the crystalline electric fields further perturb the energy levels by Stark splitting of the terms. This effect is stronger than the spin-orbit coupling and consequently equation (11) no longer applies. The crystal field effects must be calculated by a more rigid quantum mechanical calculation given in the following section.

Quantum mechanical calculations; ⁽¹⁸⁾ the perturbation Hamiltonian

In order to treat the paramagnetic problem of practical interest, we will now take a more general, if somewhat less transparent, approach

and solve the paramagnetic problem including crystal field effects, spin orbit coupling and the magnetic field simultaneously using second order perturbation theory.

A short review of perturbation theory using the Dirac notation is as follows. Consider a quantum mechanical system for which we can obtain an exact or at least a very good solution. We can write the eigenvalue equation

$$H^{\circ} |\beta\rangle = E^{\circ} |\beta\rangle, \quad (13)$$

where H° is a Hermitian operator called the Hamiltonian, E° is the energy eigenvalue of the system and $|\beta\rangle$ is the basic system eigenket where β is the degeneracy parameter. If this system is perturbed slightly by a small perturbation, ΔH , we can write the new eigenvalue equation as

$$(H^{\circ} + \Delta H) |E\rangle = E |E\rangle, \quad (14)$$

where $|E\rangle$ is the perturbed eigenket and E is the new, slightly different, energy eigenvalue. It can be shown that the perturbed eigenket, to zeroth order approximation can be written as a linear combination of the unperturbed eigenkets, (19)

$$|E\rangle^{\circ} = a_{\beta} |\beta\rangle, \quad (15)$$

where the repeated variable β implies a summation over all degenerate states β . Equation (14) can now be written as

$$(H^{\circ} + \tilde{H}) |E\rangle^{\circ} = E |E\rangle^{\circ} = (E^{\circ} + E_S) |E\rangle^{\circ}, \quad (16)$$

where E_S is the change in energy due to the perturbation. \tilde{H} is known as the perturbation Hamiltonian. It can also be shown that \tilde{H} to second order has the form (19)

$$\tilde{H} = |\beta'\rangle\langle\beta'| \left[\Delta H + \frac{\Delta H |\beta''\rangle\langle\beta''| \Delta H}{E^0(\beta) - E^0(\beta'')} \right] |\beta\rangle\langle\beta| \quad (17)$$

where β'' refers to excited states and ΔH is the specific perturbation. With the use of equation (13) and equation (15), equation (16) can be reduced to

$$\tilde{H} |E\rangle^0 = E_S |E\rangle^0 .$$

Using equation (15)

$$\tilde{H} a_\beta |\beta\rangle = E_S a_\beta |\beta\rangle . \quad (18)$$

Multiplying equation (18) by $\langle\beta'|$ gives

$$\langle\beta'|\tilde{H}|\beta\rangle a_\beta = E_S a_{\beta'} . \quad (19)$$

For an n-fold degeneracy we have n equations containing n unknown coefficients a_β . The condition for nontrivial solutions of equation (19) is

$$|\langle\beta'|\tilde{H}|\beta\rangle - E_S \delta_{\beta',\beta}| = 0 , \quad (20)$$

which gives n values of the perturbed energy E_S in terms of the perturbation Hamiltonian and the unperturbed eigenkets.

The basic problem then, is to find \tilde{H} , which will from now on be referred to equivalently as the spin Hamiltonian, H_S , and the unperturbed eigenkets $|\beta\rangle$. The perturbing effects of interest are:

$$\text{Spin-orbit coupling} \approx \lambda \bar{L} \cdot \bar{S}$$

where \bar{L} is the total angular momentum of the ground state, \bar{S} is the total spin and λ is some undetermined constant.

$$\text{Magnetic field} \approx \beta \bar{H} \cdot (\bar{L} + 2\bar{S})$$

where \bar{H} is the d.c. magnetic field and β is the Bohr magneton as previously discussed.

Crystalline field effects $\approx \sum_K U(\bar{r}_K)$ where U is $-e$ times the electrostatic potential of the crystalline field and \bar{r}_K is the position vector of the k^{th} electron. $U(\bar{r})$ will have certain space symmetries characteristic of the particular crystal structure.

In most maser applications the crystalline field effects are large in comparison to the spin-orbit coupling or the magnetic field interaction. We can therefore regard these as part of the unperturbed Hamiltonian, find the corresponding eigenkets, and then let the spin-orbit coupling and magnetic field act as perturbations to the new H^0 which contains the term $\sum_K U(\bar{r}_K)$.

Let us first choose a set of eigenkets of H^0 and a complete set of commuting observables. We will take as the observables, \bar{S}^2 , S_Z and R where R contains all the other observables needed to make the set complete. The basic eigenkets will be written as $|S M_S \rho\rangle$ where the eigenvalues of \bar{S}^2 , S_Z and R are $S(S+1)$, M_S , ρ respectively. We notice that \bar{S}^2 and \bar{S} commute with H^0 and assume that all R 's commute with H^0 as well.

It is not necessary to calculate the energy levels and eigenkets of H^0 , but only to see how the spin-orbit coupling and magnetic field remove the $2S+1$ spin degeneracy of the ground state of H^0 . We then have for the perturbation

$$\begin{aligned}\Delta H &= \bar{L} \cdot \bar{S} + \beta \bar{H} \cdot (\bar{L} + 2\bar{S}) \\ &= L_i T_i + 2\beta H_i S_i\end{aligned}\quad (21)$$

where $T_i = \lambda S_i + \beta H_i$ and the subscripts imply summation over the three coordinate axes. Using equation (17), the perturbation Hamiltonian or spin-Hamiltonian can be written as

$$\begin{aligned}H_S &= |S_g M'_g \rho_g\rangle \langle S_g M'_g \rho_g| \Delta H |S_g M_g \rho_g\rangle \langle S_g M_g \rho_g| \\ &+ \frac{|S_g M'_g \rho_g\rangle \langle S_g M'_g \rho_g| \Delta H |S_g M''_g \rho_g\rangle \langle S_g M''_g \rho_g| \Delta H |S_g M_g \rho_g\rangle \langle S_g M_g \rho_g|}{E^0(S_g \rho_g) - E^0(S_g \rho)},\end{aligned}\quad (22)$$

where S_g and ρ_g refer to ground states and S , M''_g and ρ refer to excited states. The operator \bar{S}^2 commutes with ΔH and thus ΔH is diagonal with respect to S . The only value of S that has non-zero matrix elements is then $S = S_g$. Equation (22) can be rewritten as

$$\begin{aligned}H_S &= |M'_g \rho_g\rangle \langle M'_g \rho_g| \Delta H |M_g \rho_g\rangle \langle M_g \rho_g| \\ &+ \frac{|M'_g \rho_g\rangle \langle M'_g \rho_g| \Delta H |M''_g \rho_g\rangle \langle M''_g \rho_g| \Delta H |M_g \rho_g\rangle \langle M_g \rho_g|}{E^0(\rho_g) - E^0(\rho)}.\end{aligned}\quad (23)$$

For the evaluation of equation (23) the following matrix elements will be needed:

$$\langle M'_g \rho' | S_i | M_g \rho \rangle = \delta_{\rho\rho'} \langle M'_g | S_i | M_g \rangle \quad (24)$$

$$\langle M'_g \rho' | H_i | M_g \rho \rangle = \delta_{\rho\rho'} \delta_{M_S M'_S} H_i \quad (25)$$

$$\begin{aligned}\langle M'_g \rho' | T_i | M_g \rho \rangle &= \langle M'_g \rho' | (\lambda S_i + \beta H_i) | M_g \rho \rangle \\ &= (\lambda \langle M'_g | S_i | M_g \rangle + \beta H_i \delta_{M'_S M_S}) \delta_{\rho\rho'}\end{aligned}\quad (26)$$

$$\langle M'_g \rho' | L_i | M_g \rho \rangle = \delta_{M'_S M_S} \langle \rho' | L_i | \rho \rangle.$$

Since the above matrix element must be Hermitian and purely imaginary $\langle \rho' | L_i | \rho \rangle = - \langle \rho | L_i | \rho' \rangle$. We then have

$$\langle \rho | L_i | \rho \rangle = 0 \text{ for } \rho = \rho' . \quad (27)$$

Evaluating the first term in equation (23) we obtain

$$\begin{aligned} H_S^{(1)} &= |M'_S \rho_g\rangle \langle M'_S \rho_g | 2\beta H_i S_i | M_S \rho_g\rangle \langle M_S \rho_g | \\ &= |M'_S \rho_g\rangle \langle M'_S \rho_g | 2\beta \bar{H} \cdot \bar{S} | M_S \rho_g\rangle \langle M_S \rho_g | . \end{aligned} \quad (28)$$

In order to calculate the energy corresponding to the first term of the spin Hamiltonian, equation (28) must operate on a linear combination of ground level eigenkets [see Eq. (18)]. The operator $|M_S \rho_g\rangle \langle M_S \rho_g |$ will not affect the linear combination and can thus be set equal to unity as can the operator $|M'_S \rho_g\rangle \langle M'_S \rho_g |$. The first order spin Hamiltonian then becomes

$$H_S^{(1)} = 2\beta \bar{H} \cdot \bar{S} \quad (29)$$

which is identical to the semi-classical result, equation (12), for spins.

To get the observed deviation from the pure Zeeman energy levels we must evaluate the second order term, $H_S^{(2)}$, of equation (23). We obtain from equations (21), (26), and (27)

$$\begin{aligned} \langle M'_S \rho_g | \Delta H | M''_S \rho_g \rangle \langle M''_S \rho_g | \Delta H | M_S \rho_g \rangle &= \langle M'_S \rho_g | L_i T_i | M''_S \rho_g \rangle \langle M''_S \rho_g | L_j T_j | M_S \rho_g \rangle . \\ &= q_{ij}(\rho) \langle M'_S \rho_g | T_i | M''_S \rho_g \rangle \langle M''_S \rho_g | T_j | M_S \rho_g \rangle . \end{aligned} \quad (30)$$

The term $2\beta H_i S_i$ is zero from equations (24) and (25) since ρ , which labels the excited states, is always different than ρ_g , and where

$$q_{ij}(\rho) = \langle M'_S \rho_g | L_i | M''_S \rho \rangle \langle M''_S \rho | L_j | M_S \rho_g \rangle . \quad (31)$$

If we perform the summation over M''_S and introduce equation (30) into the second term in equation (23) we obtain

$$H_S^{(2)} = |M'_S \rho_g \rangle \langle M'_S \rho_g | \frac{q_{ij}(\rho) T_i T_j}{E^0(\rho_g) - E^0(\rho)} |M_S \rho_g \rangle \langle M_S \rho_g | . \quad (32)$$

Using the same argument as in equation (29), the operators $|M_S \rho_g \rangle \langle M_S \rho_g |$ and $|M'_S \rho_g \rangle \langle M'_S \rho_g |$ do not have any effect on a combination of ground level eigenkets. We can write the result for the second order term in equation (23) as

$$H_S^{(2)} = Q_{ij} T_i T_j , \quad (33)$$

where

$$Q_{ij} = \frac{q_{ij}(\rho)}{E^0(\rho_g) - E^0(\rho)} .$$

We then have for the complete spin Hamiltonian, using equations (21), (29), and (33),

$$H_S = H_S^{(1)} + H_S^{(2)} = 2\beta \bar{H} \cdot \bar{S} + Q_{ij} (\lambda S_i + \beta H_i) (\lambda S_j + \beta H_j) . \quad (34)$$

It can be shown that Q_{ij} is a symmetric tensor and can thus be diagonalized so that the spin Hamiltonian can be written as

$$\begin{aligned}
 H_S &= 2\beta\bar{H}\cdot\bar{S} + Q_{ii} (\lambda S_i + \beta H_i)^2 \\
 &= g_{ij}\beta H_i S_j + Q_{ii} (\lambda^2 S_i^2 + \beta^2 H_i^2) .
 \end{aligned}
 \tag{35}$$

The factor 2 in the first term was introduced in the original perturbation as the gyromagnetic ratio of free spin. By adding the cross terms from $(\lambda S_i + \beta H_i)^2$ the g factor now becomes anisotropic. We will reintroduce the scalar variable g assuming the anisotropy is small.

Equation (35) becomes

$$H_S = g\beta\bar{H}\cdot\bar{S} + Q_{ii} (\lambda^2 S_i^2 + \beta^2 H_i^2) . \tag{36}$$

By omitting the H_i^2 terms, which are the same for all levels equation (36) can be written as

$$H_S = g\beta\bar{H}\cdot\bar{S} + D S_z^2 + E(S_x^2 - S_y^2) , \tag{37}$$

where the form of the last two terms results from the tetragonal crystal symmetry of the present problem. A convenient zero of energy can be made by subtracting

$D/3[S_g(S_g+1)]$ from equation (37), giving

$$H_S = g\beta\bar{H}\cdot\bar{S} + D[S_z^2 - \frac{1}{3}S_g(S_g+1)] + E(S_x^2 - S_y^2) \tag{38}$$

$$\begin{aligned}
 &= g\beta\bar{H}\cdot\bar{S} + D[S_z^2 - 1/3 S_g(S_g+1)] + 1/2E[(S_x + iS_y)^2 \\
 &\quad + (S_x - iS_y)^2] .
 \end{aligned}
 \tag{39}$$

The constants g , D , and E can be evaluated experimentally for different maser materials.

The first term in equation (38) is the familiar Zeeman term for spin states. The second term represents a quadrupole interaction with the crystalline field and the third term represents higher order interactions.

We can now return to equation (20) and solve for the energy, E_S , once the matrix elements $\langle \beta' | H_S | \beta \rangle$ are found.

In the section headed Paramagnetic Energy Levels we found that Cr^{+3} had a ${}^4F_{3/2}$ ground state, i.e., $S = 3/2$, $L = 3$, $J = 3/2$. Our ground state eigenkets are $|S_g M_S \rho_g\rangle$ with $S_g = 3/2$ so that M_S can take on the values $3/2, 1/2, -1/2, -3/2$. In the following the labels S_g and ρ_g will be understood and equation (20) can be written

$$\langle M'_S | H_S | M_S \rangle = - E_S \delta_{M'_S M_S} = 0 . \quad (40)$$

M_S can take on four values, thus equation (40) will be a 4x4 matrix whose determinant must equal zero.

The x, y, z coordinate system used is shown in Figure 4. The three orthogonal crystal symmetry axes are a, a, c , with c in the z -direction and the a -axes 45° from y in the x - y plane. The magnetic field, \vec{H} , is shown with an arbitrary incidence labeled by the angles θ and ϕ .

We will use the following definitions and results from quantum mechanics:

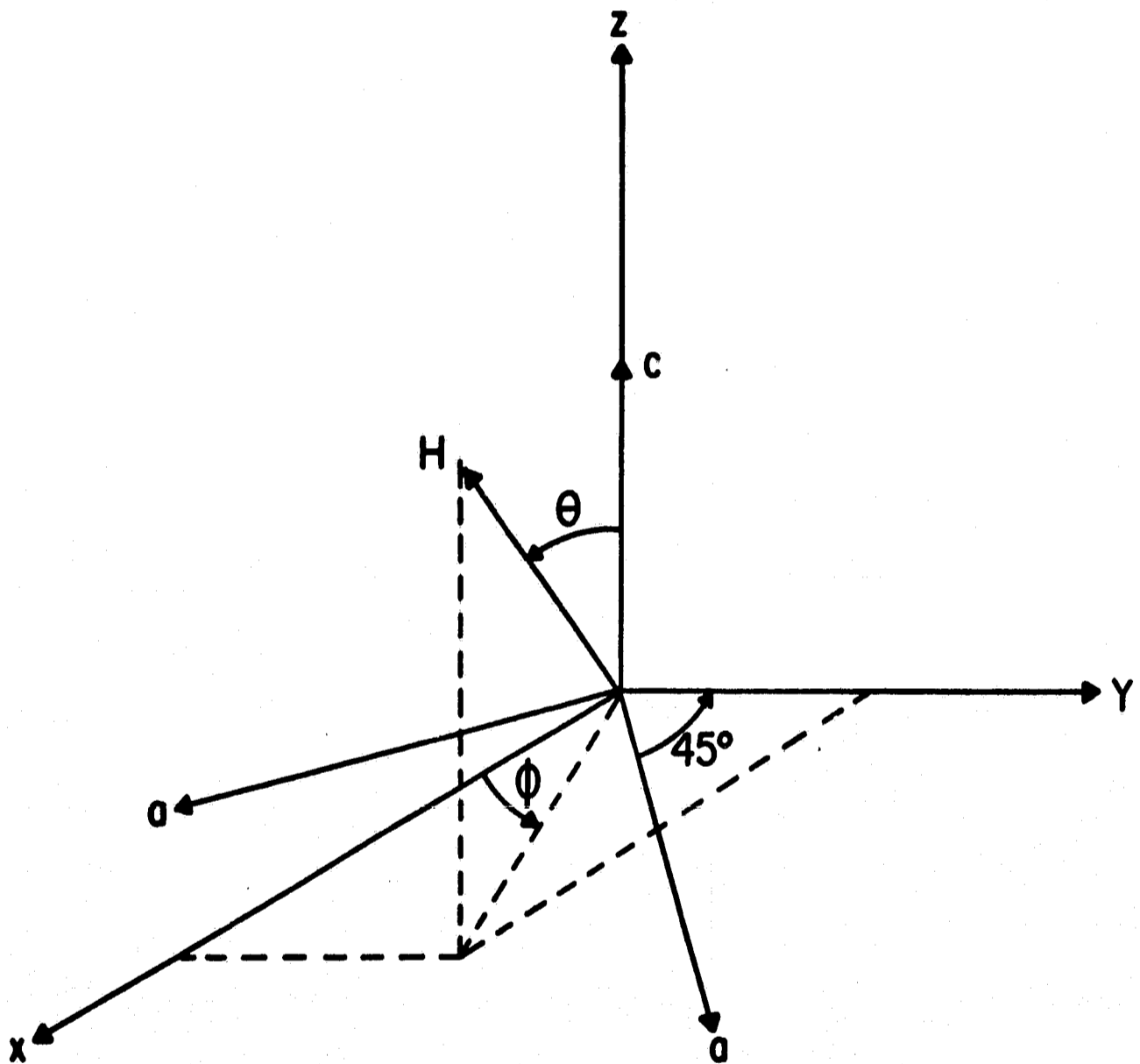


Figure 4 - Spin Hamiltonian Coordinate System for Rutile

$$S_+ = S_x + iS_y \quad (41)$$

$$S_- = S_x - iS_y \quad (42)$$

$$S_x = 1/2 (S_+ + S_-) \quad (43)$$

$$S_y = 1/2i (S_+ - S_-) \quad (44)$$

$$\langle M'_S | S_z | M_S \rangle = M_S \delta_{M'_S M_S} \quad (45)$$

$$\langle M'_S | S_{\pm} | M_S \rangle = \sqrt{S(S+1) - M_S(M_S \pm 1)} \delta_{M'_S M_S \pm 1} \quad (46)$$

$$\langle M'_S | S_x | M_S \rangle = 1/2 \langle M'_S | S_+ | M_S \rangle + 1/2 \langle M'_S | S_- | M_S \rangle \quad (47)$$

$$\langle M'_S | S_y | M_S \rangle = 1/2i \langle M'_S | S_+ | M_S \rangle - 1/2 \langle M'_S | S_- | M_S \rangle . \quad (48)$$

The first term in the spin Hamiltonian, equation (38), is $g \beta \bar{H} \cdot \bar{S}$
 $= g\beta (H_x S_x + H_y S_y + H_z S_z)$. Evaluating the $H_z S_z$ term first, using
equation (45),

$$\langle M'_S | g\beta H_z S_z | M_S \rangle = g\beta H \cos\theta \langle M'_S | S_z | M_S \rangle$$

$$= g\beta H \cos\theta M_S \delta_{M'_S M_S}$$

$$= g\beta H \cos\theta \begin{matrix} M_S = 3/2 & 1/2 & -1/2 & -3/2 \\ \left[\begin{array}{cccc} 3/2 & 0 & 0 & 0 \\ 0 & 1/2 & 0 & 0 \\ 0 & 0 & -1/2 & 0 \\ 0 & 0 & 0 & -3/2 \end{array} \right] & M'_S = 3/2 & & \\ & & & & 1/2 & & & \\ & & & & -1/2 & & & \\ & & & & -3/2 & & & \end{matrix} \quad (49)$$

The $H_{x'x}$ term is evaluated using equations (41), (42), (43), and (44);

$$\begin{aligned}
 \langle M'_S | g\beta H_{x'x} S_x | M_S \rangle &= 1/2 g\beta H \sin\theta \cos\phi \langle M'_S | S_+ + S_- | M_S \rangle \\
 &= 1/2 g\beta H \sin\theta \cos\phi (\langle M'_S | S_+ | M_S \rangle + \langle M'_S | S_- | M_S \rangle) \\
 &= 1/2 g\beta H \sin\theta \cos\phi \begin{bmatrix} 0 & \sqrt{3} & 0 & 0 \\ 0 & 0 & 2 & 0 \\ 0 & 0 & 0 & \sqrt{3} \\ 0 & 0 & 0 & 0 \end{bmatrix} + 1/2 g\beta H \sin\theta \cos\phi \begin{bmatrix} 0 & 0 & 0 & 0 \\ \sqrt{3} & 0 & 0 & 0 \\ 0 & 2 & 0 & 0 \\ 0 & 0 & \sqrt{3} & 0 \end{bmatrix} \\
 &= 1/2 g\beta H \sin\theta \cos\phi \begin{bmatrix} 0 & \sqrt{3} & 0 & 0 \\ \sqrt{3} & 0 & 2 & 0 \\ 0 & 2 & 0 & \sqrt{3} \\ 0 & 0 & \sqrt{3} & 0 \end{bmatrix} .
 \end{aligned} \tag{50}$$

The same procedure is carried out on each term in the spin Hamiltonian, equation (38), noting that

$$\langle M'_S | S_z^2 | M_S \rangle = \langle M'_S | S_z | M''_S \rangle \langle M''_S | S_z | M_S \rangle$$

and
$$\langle M'_S | S_{\pm}^2 | M_S \rangle = \langle M'_S | S_{\pm} | M''_S \rangle \langle M''_S | S_{\pm} | M_S \rangle .$$

When all the matrix elements in the secular determinant, equation (40), have been evaluated by the above procedure the determinant can be expanded into a fourth order polynomial in E_S with g , β , D , and E as constants to be evaluated experimentally and H , θ , and ϕ as parameters.

The secular equation becomes⁽²¹⁾

$$\begin{aligned}
 E_S^4 - E_S^2 (5/2h^2 + 2D^2 + 6E^2) + E_S h^2 (2D - 6D \cos^2 \theta - 6E \sin^2 \theta \cos 2\phi) \\
 + 9/16h^4 + 1/2 h^2 (D^2 - 6D^2 \cos^2 \theta + 9 E^2 \cos 2\phi) \\
 + 12 DE \sin^2 \theta \cos 2\phi + (D^2 + 3E^2)^2 = 0
 \end{aligned}
 \tag{51}$$

where $h = g\beta H$.

The four roots of equation (51) give the four energy levels corresponding to those given by equation (12) but modified by the crystal field effects and the orientation of the magnetic field with respect to the crystal symmetry axes.

The constants in equation (51) are given by Gerritsen⁽²¹⁾ as

$$D = 16.6 \text{ GHz}$$

$$E = 8.07 \text{ GHz}$$

$$h = g\beta H = 2.75 \text{ H GHz/kilogauss.}$$

Equation (51) was solved by Bairstow's method of finding the roots of a general fourth order polynomial. The solution was programmed for an IBM 7074 computer with H , θ and ϕ as inputs and the resonance frequencies, i.e., $E_S(M_S) - E_S(M'_S)$ in GHz as the output. A complete program was written in a modified Fortran II language called Daft (see Appendix I).

The energy levels for a particularly significant magnetic field orientation are given in Figure 5. The most striking difference between the Zeeman effect and Figure 5 is the splitting of the energy levels with no magnetic field applied. This is primarily due to a Stark

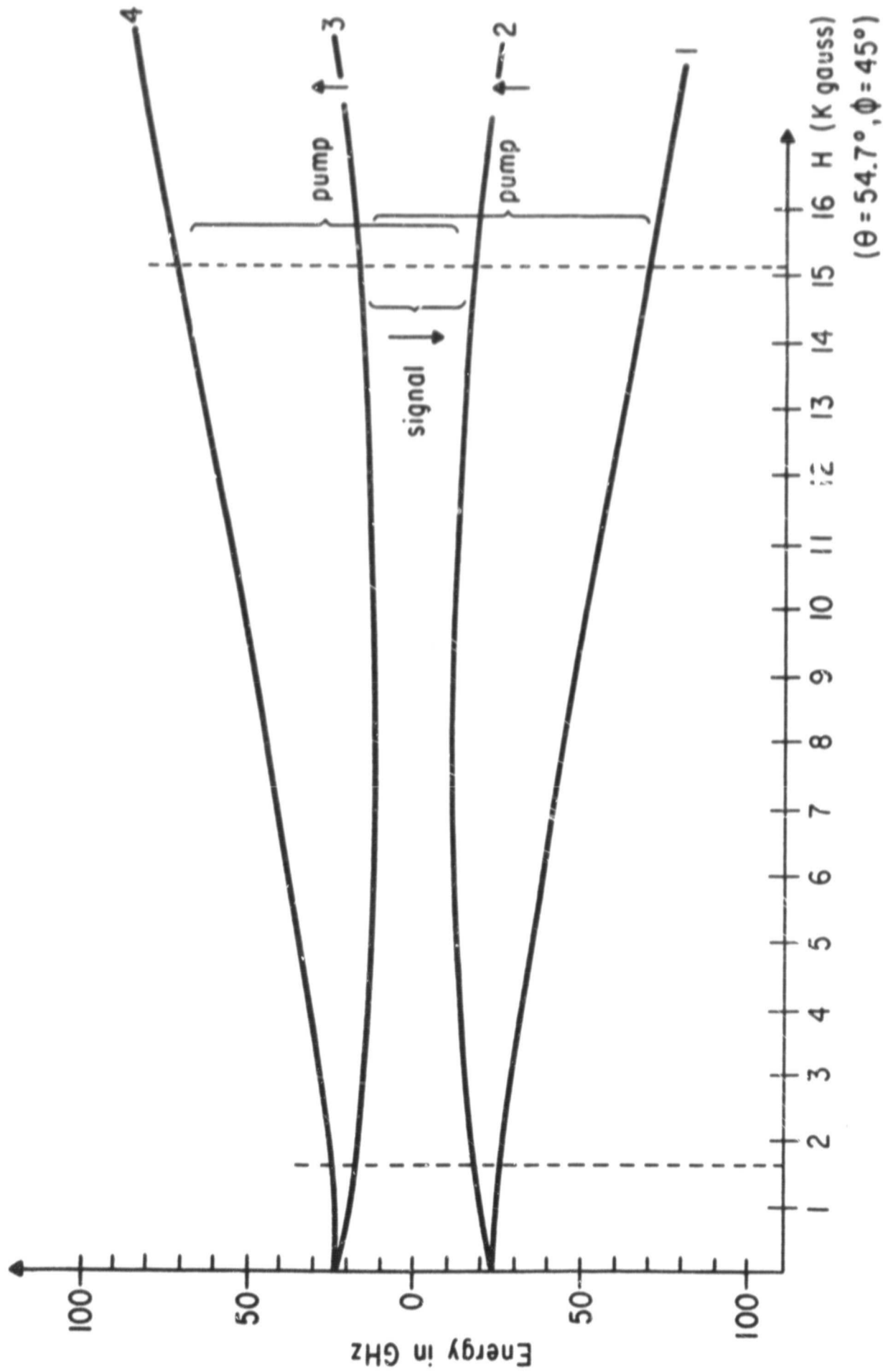


Figure 5 - Push-pull Energy Levels in Rutile

effect from the crystalline electric fields. For very large values of H the energy levels are dominated by the term $g\beta\bar{H}\cdot\bar{S}$ in the spin Hamiltonian and approach a normal Zeeman diagram.

Having found the energy levels of Cr^{+3} we will now see how these levels are populated when in thermal equilibrium and in contact with various radiation fields.

Einstein A and B coefficients and radiation

Consider a system of a large number of atoms in thermal equilibrium. The discrete energy levels of an atom are designated by E_1, E_2, \dots, E_n etc. where $E_1 < E_2 < \dots < E_n$. The total energy will be distributed among the various energy levels according to a Boltzmann distribution; i.e.,

$$N_i = K \exp(-E_i/kT) \quad (52)$$

where N_i is the number of atoms in the i^{th} energy level E_i , k is Boltzmann's constant and K is independent of i for nondegenerate levels. (See equation 8).

Let this system now be in equilibrium with a radiation field $\rho(\nu)$, following the Planck law

$$\rho(\nu) = 8\pi \frac{h\nu^3}{c^3} \frac{1}{\exp(h\nu/kT) - 1} \quad (53)$$

If the radiation in the frequency interval $d\nu$ is centered at $\nu = \nu_{12}$ where $E_2 - E_1 = h\nu_{12}$, there will be an absorption of energy and a corresponding change in the population distribution. The time rate of change of N_2 due to absorption is

$$\left. \frac{dN_2}{dt} \right|_{\text{abs}} = B_{12} \rho(\nu) N_1 . \quad (54)$$

B_{12} is called the Einstein coefficient of absorption.

There are two ways in which level two can decrease in population. The first is stimulated emission where the rate of change of N_2 is

$$\left. \frac{dN_2}{dt} \right|_{\text{sti.Em.}} = - B_{21} \rho(\nu) N_2 . \quad (55)$$

B_{21} is called coefficient of stimulated emission. The second downward process is independent of the radiation field and is called spontaneous emission. The rate equation is

$$\left. \frac{dN_2}{dt} \right|_{\text{spo.Em.}} = - A_{21} N_2 , \quad (56)$$

where A_{21} is the coefficient of spontaneous emission. Combining equations (54) to (56) one obtains

$$\left. \frac{dN_2}{dt} \right|_{\text{Total}} = B_{12} \rho(\nu) N_1 - [A_{21} + B_{21} \rho(\nu)] N_2 . \quad (57)$$

When the system is in equilibrium with the radiation field the upward transitions must be equal to the downward transitions; thus, equation (57) must equal zero. Solving for $\rho(\nu)$ and making use of the Boltzmann law, equation (57) becomes

$$\rho(\nu) = \frac{A_{21}}{B_{12} \exp(h\nu_{21}/kT) - B_{21}} . \quad (58)$$

Direct comparison of equations (58) and (53) show that $B_{21} = B_{12}$ and

that

$$\frac{A_{21}}{B_{21}} = \frac{8\pi h\nu^3}{c^3} , \quad (59)$$

if it is assumed that A_{21} , B_{21} and B_{12} are atomic properties and thus independent of the temperature.

From equation (59) we conclude that spontaneous emission is usually only important at infrared and higher frequencies. In the microwave region A_{ij} can be neglected in the rate equations. It will be important only in its effect on the ultimate noise figure of the maser.

Equation (57) can now be written as

$$\frac{dN_2}{dt} = B_{12}\rho(\nu)(N_1 - N_2). \quad (60)$$

From inspection of equation (60) it can be seen that radiation is being absorbed as long as $N_1 > N_2$. When $N_1 = N_2$ radiation is no longer absorbed and the levels are said to be saturated. If, by some method N_2 could be made larger than N_1 , the radiation field would stimulate emission ($\frac{dN_2}{dt} < 0$) until N_2 again equalled N_1 . The requirement $N_2 > N_1$ is called population inversion and is necessary for maser operation. If equation (52) is applied to an inverted state, we have

$$\frac{N_2}{N_1} > 1 \rightarrow \frac{\exp(-E_2/kT)}{\exp(-E_1/kT)} = \exp\left(\frac{E_1 - E_2}{kT}\right) > 1 .$$

Since $E_2 > E_1$, the temperature T must be less than zero. A population inversion is then said to have a negative spin temperature. We need not worry about the physical interpretation of a "negative

temperature," since T is defined in thermodynamics as simply one of the constants which appears in the Boltzmann expression for the energy distribution normally found in ordinary systems. It usually corresponds to our intuitive notions of hot and cold. If we force an energy distribution on the system which is non-Maxwell-Boltzmann, we cannot expect the constant T to have the same physical meaning.

We will now see how a population inversion is maintained in the three level maser scheme.

The Three Level Maser (Bloembergen⁽²²⁾)

Take a three level system in thermal equilibrium such as that shown in Figure 3a. Apply a strong signal, $\rho(\nu_{13})$, to the 1-3 transition. This will be called the pump signal. As in the description of equation (60), pump energy will be absorbed until $n_1 = n_3 = 1/2(N_1 + N_3)$. Hereafter, small case n will denote instantaneous populations and N will denote population at thermal equilibrium. With the pump applied, a population similar to that shown in Figure 3b will result. It is easily seen that a population inversion exists between levels 2 and 3. A weak signal applied to the 2-3 transition will stimulate emission from level 3 to level 2. (A weak signal is a signal small enough that its stimulated transitions do not seriously affect the population inversion.)

Before writing the complete rate equations, we must define a relaxation process such that when the radiation fields are turned off the system will return to thermal equilibrium by some non-radiative process in a time T . In the case of paramagnetic ions

in a crystal lattice the most important relaxation process is spin-lattice relaxation, where a spin exchanges a quantum of energy with the lattice thermal vibrations. Let us define a relaxation probability, $w_{ij} \propto \frac{1}{T}$. In analogy to equation (54-57), relaxation rate equation can be written as

$$\begin{aligned} \frac{dn_1}{dt} &= -w_{12}n_1 + w_{21}n_2 \\ \frac{dn_2}{dt} &= w_{12}n_1 - w_{21}n_2 \end{aligned} \quad (61)$$

At thermal equilibrium $\frac{dN_1}{dt} = \frac{dN_2}{dt} = 0$, thus

$$\frac{w_{12}}{w_{21}} = \frac{N_2}{N_1} = \exp\left(\frac{E_1 - E_2}{kT}\right) \quad (62)$$

We can now write the three-level rate equations;

$$\begin{aligned} \frac{dn_3}{dt} &= (w_{13}n_1 - w_{31}n_3) + (w_{23}n_2 - w_{32}n_3) \\ &\quad + (B_{13}\rho_{13}n_1 - B_{31}\rho_{13}n_3) + (B_{23}\rho_{23}n_2 - B_{32}\rho_{23}n_3) \\ \frac{dn_2}{dt} &= (w_{32}n_3 - w_{23}n_2) + (w_{12}n_1 - w_{21}n_2) + (B_{32}\rho_{23}n_3 - B_{23}\rho_{23}n_2) \end{aligned} \quad (63)$$

$$\frac{dn_1}{dt} + \frac{dn_2}{dt} + \frac{dn_3}{dt} = 0$$

$$n_1 + n_2 + n_3 = N$$

where

$$\rho_{ij} \equiv \rho(\nu_{ij}) \quad (64)$$

At 4°K and a frequency of 36 GHz, $h\nu/kT = 0.4$; thus, $\exp(h\nu/kT)$ can be expanded with reasonable accuracy as $\exp(h\nu/kT) = 1 + h\nu/kT$.

We have also assumed that the pump radiation is much stronger than the signal; i.e., $\rho_{13}B_{13} \gg B_{23}\rho_{23}$. The set of equations (63) can then be solved for $(n_3 - n_2)$.

$$(n_3 - n_2) = \frac{hN}{3kT} \frac{w_{12}\nu_{12} - w_{23}\nu_{23}}{w_{12} + w_{23} + B_{32}\rho_{32}} \quad (65)$$

the net stimulated emission power from the 2-3 transition is given by

$$\begin{aligned} P &= h\nu_{32} (B_{32}\rho_{32} n_3 - B_{23}\rho_{23} n_2) \\ &= h\nu_{32} B_{32}\rho_{32} (n_3 - n_2). \end{aligned} \quad (66)$$

Combining equations (65) and (66),

$$P = \frac{N h^2 \nu_{32}}{3kT} \frac{(w_{12}\nu_{12} - w_{23}\nu_{23}) B_{32}\rho_{32}}{w_{12} + w_{23} + B_{23}\rho_{23}}$$

Assume all w_{ij} 's between different levels are equal, which seems experimentally justified, and $\rho_{23}B_{23} \ll w_{12}$ which is true for weak signals. Then

$$\begin{aligned} P &= \frac{Nh^2}{6kT} (\nu_{21} - \nu_{32}) B_{32} \rho_{32} \nu_{32} \\ \text{and so } P &= \frac{Nh^2}{6kT} (\nu_{31} - 2\nu_{32}) B_{32} \rho_{32} \nu_{32}. \end{aligned} \quad (67)$$

The essential features of the operation of a 3-level maser can be seen in equation (67). First of all, the power output, P , is directly proportional to the signal radiation density, $\rho(\nu_{23})$. Higher frequency operation and greater spin density give increased output, low temperature is desirable (actually essential) and finally the pump frequency must be more than twice as high as the signal frequency. The latter requirement is somewhat relaxed in the

case of a four level maser with its possibility of a more complicated pumping scheme. Equation (67) does not contain a term for pump power since it is assumed in the derivation that $\rho_{13}B_{13}$ is large enough to saturate the 1-3 transition in the presence of a weak signal.

The traveling wave maser

Early maser amplifiers were almost exclusively of the cavity type. However, we will be concerned only with the traveling wave maser. The latter has the advantage of having a lower noise figure, better gain stability, easy frequency tuning, and no fixed gain-bandwidth product.

In a traveling wave amplifier, the incoming wave is slowed by some means such as a comb structure, meander line, etc. Slowing of the input wave gives the signal a longer time in which to interact with the spin system. Equivalently, there are more wavelengths in the traveling wave amplifying section, in effect making this section electrically longer. Possibly the most simple slowing mechanism is dielectric slowing, where a waveguide is filled with a dielectric material. The slowing factor is proportional to (dielectric constant)^{1/2}. Rutile has a very high dielectric constant and low loss tangent which makes it a good candidate for dielectric slowing.

This type of slow wave structure can be as broad banded as the waveguide; thus, tuning over this range is possible as long as the energy levels and pump frequency can accommodate this change.

The gain of a traveling wave maser is given by Siegman⁽²³⁾ as

$$G(\text{db}) = 27.3 \frac{SL}{Q_m}, \quad (68)$$

where S = slowing factor = $\frac{\text{velocity of light}}{\text{group velocity}} \propto \sqrt{\epsilon}$

L = length of circuit in free space wavelengths,

Q_m = magnetic Q ,

$$\begin{aligned} \frac{1}{Q_m} &= \frac{2g^2 \beta^2 \mu_0}{h} \cdot \frac{h\nu}{kT} \cdot \frac{N}{n} \cdot \frac{I\sigma^2 n}{\Delta f_L} \\ &= 10^{-10} \frac{\nu(\text{GHz})}{20T} \cdot \frac{N}{n} \cdot \frac{I\sigma^2 n}{\Delta f_L}, \end{aligned} \quad (69)$$

and where $\nu(\text{GHz})$ = signal frequency in GHz

T = operating temperature (usually 4°K)

N = total number of spins/unit volume ($\approx 10^{19}/\text{cm}^3$)

n = number of energy levels (4 in the case of Cr^{+3})

I = inversion ratio ($\approx \frac{\nu_{\text{pump}}}{2\nu_{\text{sig}}} - 1$) for 3 levels,

$(\nu_p/\nu_s - 1)$ for push-pull pumping

σ = transition probability (≈ 1 for adjacent levels)

η = filling factor ($\approx 1/2$ for fully filled waveguide)

Δf_L = magnetic resonance linewidth (2.8 MHz/g·ΔH).

III. THE 36 GHz TRAVELING WAVE MASER

A. Design Requirements for Intended Use in Radio Astronomy

The maser amplifier's intended purpose is to be an r.f. pre-amplifier for a conventional radiometer. The gain, bandwidth, frequency, and noise figure of the maser must be made to optimize the operation of the complete system.

The center frequency was chosen to be in the 8 mm atmospheric window to minimize atmospheric attenuation and the noise contribution from the atmosphere. A center frequency of 36 GHz with the desirability of a few gigahertz tuning on either side was selected.

From equation (6), it is seen that a wide bandwidth is desirable to minimize ΔT . The bandwidth can be widened somewhat over the natural resonance linewidth by using an inhomogeneous d.c. magnetic field. However, in the gain expression, equation (69), Δf enters into the denominator and directly reduces the total gain per unit length. To regain the gain lost by broadbanding, the total length could be increased. However, the length of the slowing structure is restricted for other reasons; thus, it was decided to use the natural resonance linewidth as is. The linewidths for Cr^{+3} in rutile are quite wide, approximately 75 MHz.

The most flexible design variable is the gain, which is related to the noise figure of both the maser and the following radiometer. The effective noise temperature for amplifiers in series is given by Van Voorhis⁽²⁵⁾ as

$$T_e = T_1 + \frac{T_2}{G_1} + \dots \quad (70)$$

where T_n and G_n are the effective noise temperature and gain of the n^{th} amplifier. The first stage noise, T_1 , includes not only the intrinsic noise of the maser (which can almost be neglected) but also the noise contribution of the input waveguide, Dicke switch (if used), antenna, antenna side and back lobes, atmospheric noise and any extraneous man made noise as well. Good estimates of these noise contributions plus the noise of a second stage superhetrodyne receiver are as follows:

T_1	
zenith sky	20°K
antenna	5°K
input waveguide	50°K
maser	<u>4°K</u>
total	79°K

T_2	
11 db receiver	3500°K .

A first stage gain of 20 db reduces the second stage noise contribution to 35°K. Increasing the maser gain over 20 db does not significantly decrease the total system noise temperature. Therefore, the design criterion was to achieve as close to 20 db of gain as practical.

B. Specific Maser Design

Active material

The choice of paramagnetic ion and host lattice for use at millimeter wavelengths is somewhat simpler than at lower frequencies since there are fewer choices.

For purely practical reasons, only the hard, gem-like crystals are used for maser applications. Crystals which cannot take thermal shock, are water soluble, or have high microwave losses are clearly undesirable. The crystals must be available in pure form and accept the above paramagnetic ions as impurities.

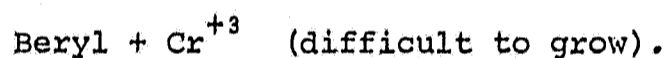
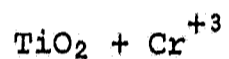
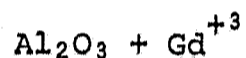
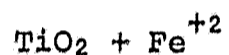
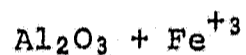
By far the most widely used crystal is sapphire (Al_2O_3), which, when doped with Cr^{+3} , becomes a ruby.

However, at millimeter wavelengths there is another consideration, that of zero field splitting (ZFS). As shown previously, the crystal field effects split the ground state with no magnetic field applied. If the zero field splitting is of the order of the signal frequency, a relatively weak magnetic field will be all that is required to produce the necessary energy level splitting. If the ZFS is small, a large field will be necessary to split the levels to something greater than the signal frequency. The effect of this strong magnetic field is to uncouple the spins from each other and produce pure spin states for which the selection rule $\Delta S = 1$ is in effect. Thus, only adjacent transitions can be made and the 3-level maser scheme will not work.

From this follows a rule of thumb that the operating frequency should not be larger than the ZFS.

Ruby, the most commonly used maser material, has a zero field splitting of only 11.5 GHz; hence, is generally not suitable for millimeter wave use.

Of the easily grown gem crystals and usable ions, we have the following combinations with sufficient zero field splitting:



Rutile (TiO_2) has a published dielectric constant on the order of 200 which makes dielectric slowing practical. (It was later determined to be considerably lower at 36 GHz.) Al_2O_3 has a dielectric constant near 10 and would require some additional slowing such as a meander line, which would be extremely difficult to fabricate to the small dimensions required. Choosing rutile because of its large dielectric constant still leaves a choice between Fe^{+3} and Cr^{+3} . The iron ion has a spin of 5/2 giving six energy levels while Cr^{+3} has a 3/2 spin and four levels. According to equation (69), Cr^{+3} should have a higher gain and the danger of cross relaxation effects from the unused energy levels is minimized. The final choice of maser material becomes Cr^{+3} in a host lattice of TiO_2 (rutile).

Crystal orientation and energy levels

Cr^{+3} has four Zeeman levels, all of which are available for signal or pump transitions. We could simply choose three of these levels and use the Bloembergen 3-level maser scheme while ignoring the fourth level. Referring to Figure 5, maser action could be achieved by pumping from level 1 to level 3 and using the 3-2 transition as a signal. However, the 3-2 inversion can be further increased by also pumping out of level 2 into level 4. This pumping method, called push-pull pumping, is particularly advantageous if the 1-3 transition can be made equal to the 2-4 transition so that a single pump frequency can be used. Inspection of the secular equation, equation (51), shows that if the term linear in E_S is zero then the equation has the form

$$E_S^4 + E_C^2 (A+B) + AB = (E_S^2 + A) (E_S^2 + B) = 0$$

and $E_S = \pm\sqrt{A}$ and $\pm\sqrt{B}$. That is, the roots are equally displaced above and below the zero level. Setting the linear term in equation (51) equal to zero we have

$$\cos 2\phi = \frac{D}{E} \left(\frac{1}{3 \sin^2\theta} - \frac{\cos^2\theta}{\sin^2\theta} \right) . \quad (71)$$

To find a unique value for ϕ and θ we must refer to the symmetry properties of the TiO_2 crystal. ⁽²⁶⁾ (A more detailed description of the crystal lattice is given in Appendix II). Rutile is a tetragonal crystal in which the Cr^{+3} ions reside in two non-equivalent sites in the unit cell. These sites are related by a 90° rotation about the

crystallographic c-axis. When the magnetic field is in the a-c plane ($\phi = 45^\circ$ in Figure 4), the two sites become equivalent. Thus, all the Cr^{+3} ions can be used for amplification rather than only one-half of the ions. Using $\phi = 45^\circ$ in equation (71) gives $\cos \theta = \sqrt{1/3}$ or $\theta = 54.7^\circ$. These are then the angles for push-pull pumping and double ion site operation. Figure 5 is a plot of these energy levels versus magnetic field. The pump and signal transitions are also indicated in Figure 5.

There are two values of H for which the signal transition equals 36 GHz. One is at 1.7 kgauss, the other at 15.1 kgauss. The high field region has a considerably higher pump frequency and thus, a higher gain as seen from equation (67).

The operating parameters are summarized below:

Push-pull pumping	$\theta = 54.7^\circ$
Double ion site operation	$\phi = 45^\circ$
High field region	$H = 15.1$ kgauss
Signal frequency	$\nu_{23} = 36.0$ GHz
Pump frequency $\nu_{13} = \nu_{24}$	$= 90.0$ GHz.

Slow wave structure

The dielectric constant of rutile at 4.2°K and 10^8 Hz is given by Sabisky⁽²⁷⁾ as

$$\epsilon = 155; \perp \text{ to crystal c-axis}$$

$$\epsilon = 255, \parallel \text{ to crystal c-axis.}$$

The waveguide coordinates are x , y , and z , with propagation being in the y -direction. The magnetic field must be in the z -direction for a reason to be stated later. The three orthogonal crystal symmetry axes a , a , and c are related to H by the angles θ and ϕ (see Figure 4).

The two values of the dielectric constant define the major and minor axes of an ellipsoid of rotation about the c -axis. The dielectric constant in any direction is just the length of the vector to the surface of the ellipsoid. It is a simple problem in geometry to show that the dielectric constant in any direction is given by

$$\epsilon = \frac{\epsilon_{\perp} \epsilon_{\parallel}}{(\epsilon_{\parallel}^2 \sin^2 \theta + \epsilon_{\perp}^2 \cos^2 \theta)^{1/2}} \quad (72)$$

where θ is the angle between the crystal c -axis and the desired direction vector. Using the given values for ϵ_{\perp} and ϵ_{\parallel} , we obtain from equation (72)

$$\begin{aligned} \epsilon_x &= 155 \\ \epsilon_y &= 204 \\ \epsilon_z &= 174. \end{aligned} \quad (73)$$

The dimensions of the dielectric filled guide can now be determined, since minimum attenuation for the dominant $TE_{1,0}$ waveguide

mode occurs at the point where the next modes, the $TE_{2,0}$ and $TE_{0,1}$, just reach cutoff. (28) In practice, the guide is made slightly smaller than this so there is no possibility of higher order modes propagating. The cutoff wavelength for the $TE_{2,0}$ mode is

$$\lambda_c = a \sqrt{\epsilon_x}$$

and for the $TE_{0,1}$

$$\lambda_c = 2b \sqrt{\epsilon_z} \quad (74)$$

where a and b are the broad and narrow dimensions of the waveguide, respectively. At 36 GHz, the free space wavelength is 8.3 mm and a and b become

$$a = 0.670 \text{ mm}$$

$$b = 0.315 \text{ mm} .$$

The slowing factor, S , is given by

$$S = \frac{c}{v_g} = \epsilon_y \left(\epsilon_y - \left(\frac{\lambda}{2a} \right)^2 \right)^{-\frac{1}{2}} \quad (75)$$

Substituting the above values into equation (75) gives

$$S = 16 .$$

When using $S = 16$ in the expression for the gain of a traveling wave maser equation (68), we obtain $G = 5.3 \text{ db/cm}$. The rutile loaded waveguide must then be approximately 4 cm long to produce 20 db of gain and have a cross section of approximately $0.07 \times 0.03 \text{ cm}$.

There is one other important property of the slow wave structure that involves the manner in which the r.f. magnetic field interacts with the spins. It was mentioned previously that the spins precess about the d.c. magnetic field with frequency ν and can interact with the r.f. field only if the r.f. field has the same ν and the same sense of circular polarization. The dominant $TE_{1,0}$ mode has two regions of circularly polarized magnetic field confined to the x-y plane as shown in Figure 6. The field has one sense of circular polarization in one half of the guide and the opposite polarization in the other half of the guide. If propagation is normally in the -y direction in Figure 6, there will be no spin interaction in the left half of the guide since the spins and the r.f. field have opposite circular polarization. It makes no difference if this half of the waveguide contains pure rutile with no Cr^{+3} doping. However, for a wave traveling in the +y direction, the sense of r.f. circular polarizations are reversed and the portion of the guide with the same polarization as the spins now contains no spins and hence cannot amplify. The net result is that the maser amplifier can amplify in only one direction or is unidirectional. It cannot break into regenerative oscillations due to some finite reflection at the ends of the slow wave structure. Frequently the waveguide modes are not sufficiently pure to make the reverse gain zero. In this case additional isolation by the use of ferrite material is required. It was decided at this stage of the design that no ferrite isolation would be used unless the maser actually oscillated.

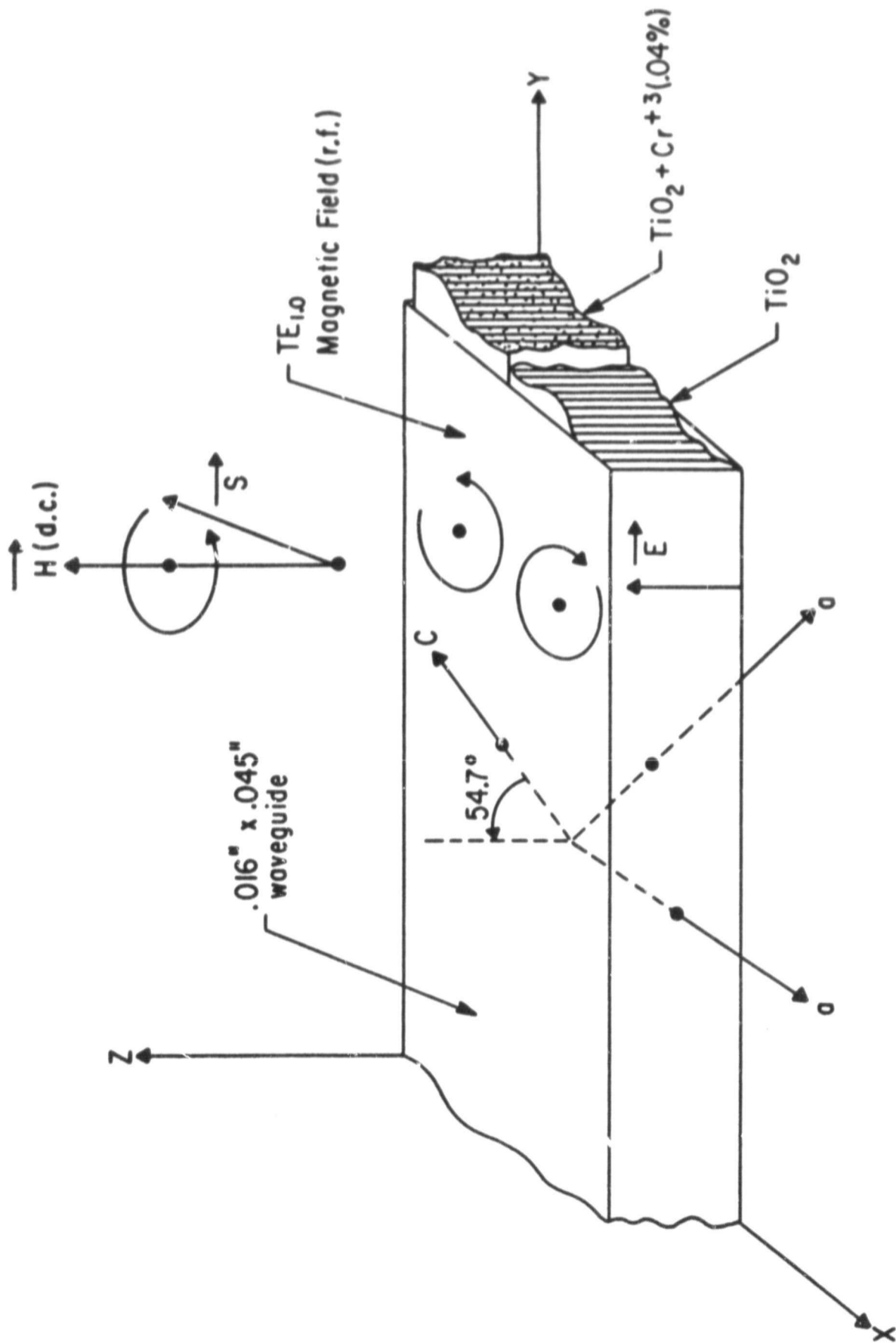


Figure 6 - 36 GHz Slow Wave Structure

C. Experimental Apparatus

The equipment used for testing and evaluating various maser configurations is shown in Figure 7. The individual components are discussed below.

Description of cryogenics system

The helium dewar is a standard, 54 inch, open neck type with a working capacity of approximately 15 liters of liquid helium. Filling is accomplished by transferring from a 50-liter storage dewar through a vacuum insulated transfer tube using compressed helium gas regulated to about 0.5 lb/in^2 . The dewar is pre-cooled with liquid nitrogen and then the nitrogen is pumped out of the inner dewar back into storage. Care must be taken to purge all condensable vapors from the waveguide prior to cooling, since water and liquid nitrogen are both lossy at millimeter wavelengths.

Description of superconducting magnet

The helium dewar and superconducting magnet were purchased as a unit from Magnion, Incorporated. The magnet is a solenoid 3.0 inches long with a 1.5 inch inside diameter. The maximum field at the center of the solenoid is 26 kgauss at a current of 29 amperes.

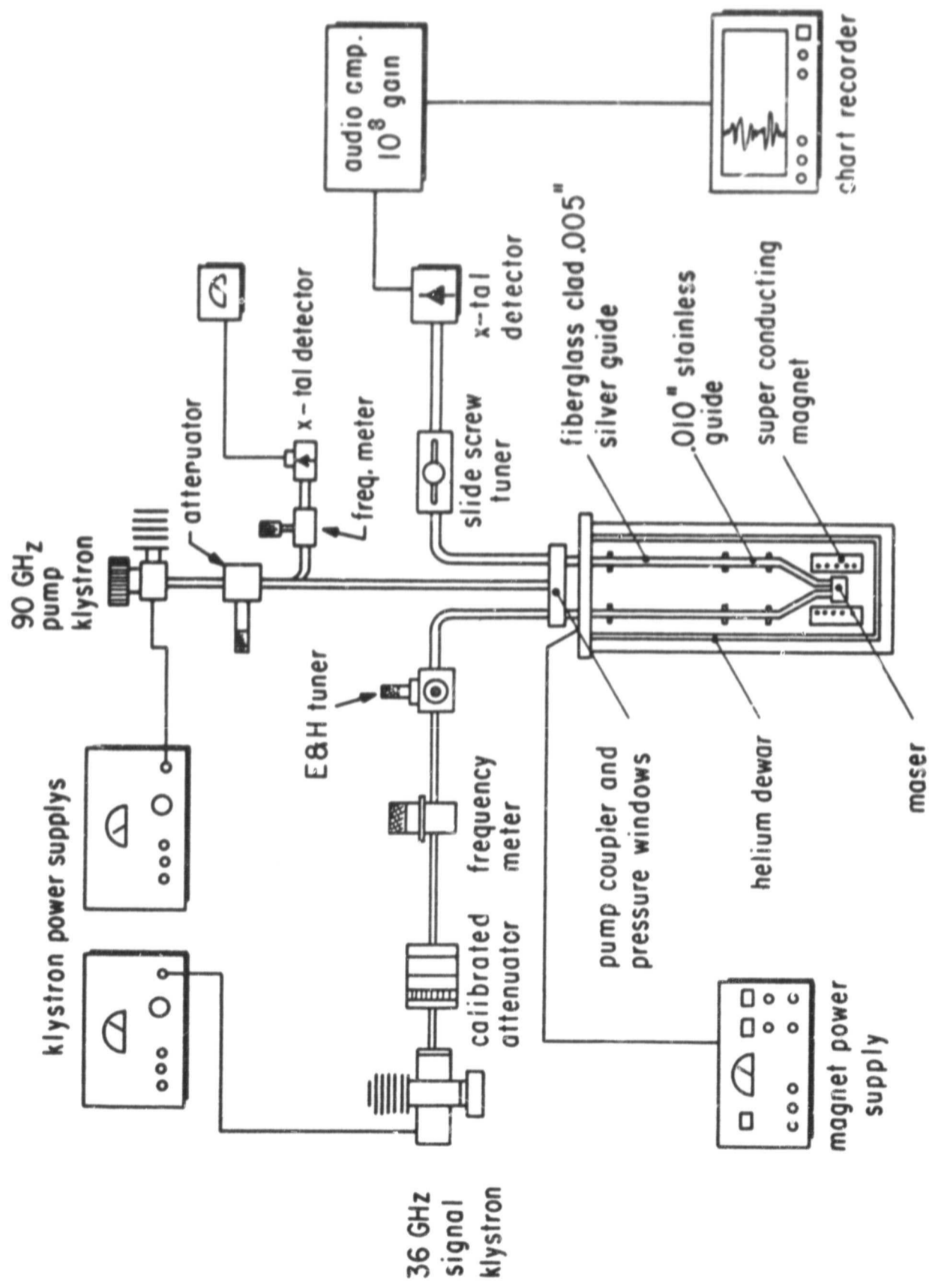


Figure 7 - Experimental Apparatus for Maser Testing

In the persistent mode of operation, the magnet is shorted internally after the field is built up by means of the external power supply. The current then circulates through the magnet and short circuit and the power supply can be disconnected. The magnetic field will persist as long as the magnet remains superconducting and no energy is extracted from the field.

The magnet power supply is designed to deliver 30 amperes into a zero resistance load. This is accomplished by using a 6-volt automobile battery as the source and a bank of transistors in series with the magnet to regulate the current. The control voltage on the transistor bases is programmed by a small clock motor so that the magnet current can be changed slowly and uniformly. The power supply also contains provisions for the persistent current switch, helium level gauge, and a battery charger to recharge the automobile battery. Figure 8 is a schematic representation of the magnet system.

The magnet is supported on a gymbal system which is adjustable from outside the dewar. This allows small corrections to be made in the angular relationship between the magnetic field and the slow wave structure.

Description of microwave hardware

The 36 GHz waveguide used is standard RG-(96)/U made from coin silver for minimum attenuation. There are two short sections of stainless steel guide with an 0.010 inch wall thickness near the middle of the helium dewar, acting as a heat block into the liquid

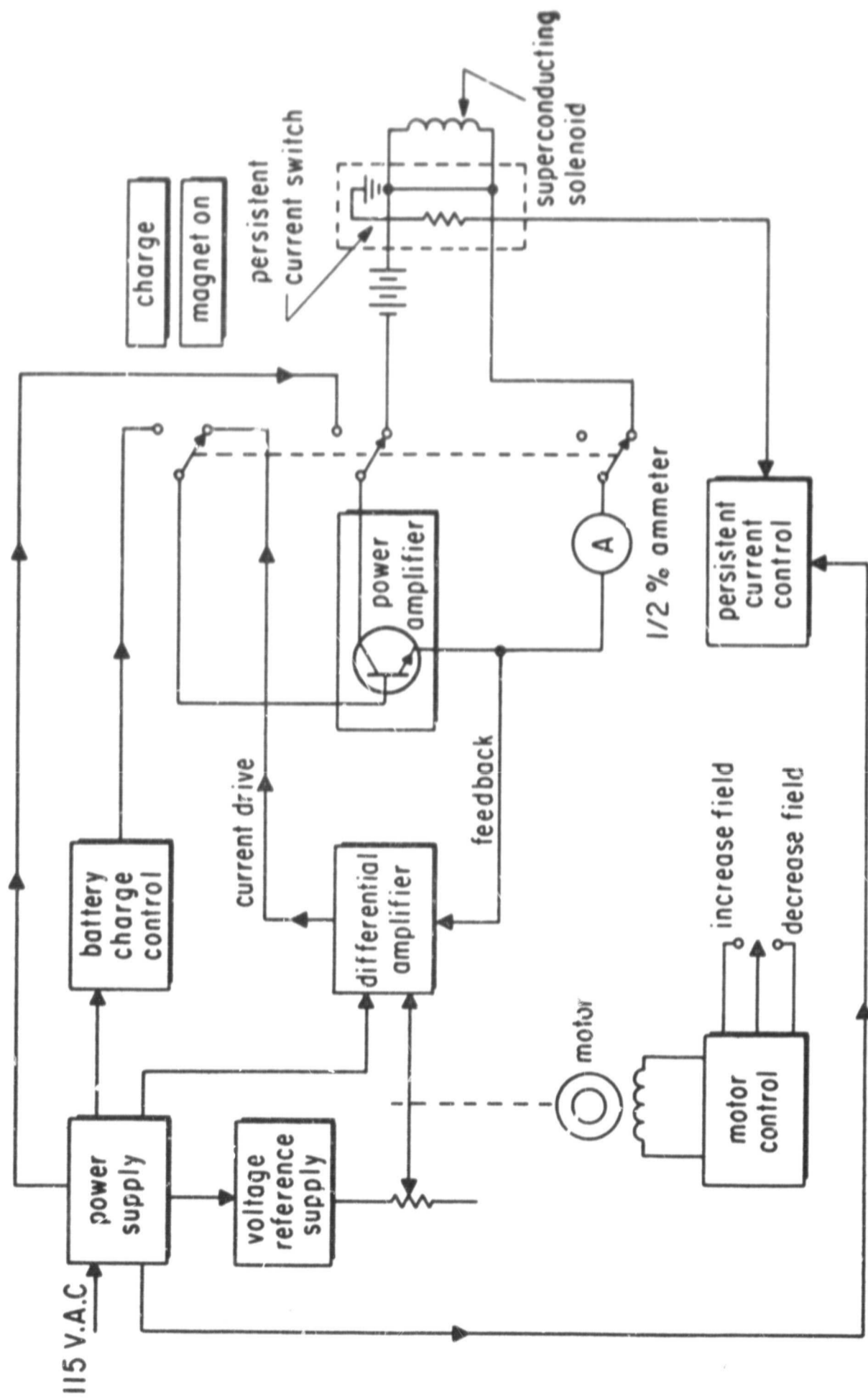


Figure 8 - Superconducting Magnet System

helium. The guide in the upper portion of the dewar is 0.005-inch wall thickness silver with fiberglass reinforcing on the outside. The fiberglass waveguide has a thermal conductivity about one-tenth that of the standard guide and the stainless has about one-fiftieth that of the standard waveguide.

On both the input and the output waveguides from the dewar there is a tuner to cancel any mismatch which may exist in the maser.

At the input is a low power klystron, tunable from 28 to 39 GHz. A precision attenuator follows the klystron so that precise input power measurements can be made. The klystron is square wave modulated at 1000 Hz, so that an audio amplifier can be placed after the crystal detector at the output. The maser is a low level device designed to amplify very low level signals; thus, a great deal of amplification is needed at the output for presentation on a chart recorder. The crystal detector, audio amplifier and chart recorder actually form a crystal video receiver which has a sensitivity of approximately -50 dbm (db below one milliwatt).

The 90 GHz pump energy comes from an Oki 90 VII klystron which has a maximum output of 70 milliwatts. The tuning range of this klystron is 85-96 GHz. The 90 GHz waveguide is WR(10) also made from silver. A frequency meter and uncalibrated attenuator are connected after the pump klystron. The pump waveguide then goes into a 3 db coupler which couples the pump energy into both the maser input and output waveguide. This insures pump saturation along the complete length of the slow wave structure. The coupler also contains pressure

windows and a fitting such that the waveguide inside the dewar can be purged, pressurized, or evacuated as necessary.

The total 36 GHz waveguide loss, apart from the maser itself, is approximately 3 db. The stainless guide contributes 1.2 db to this attenuation. The stainless steel waveguide can be gold or silver-plated or be replaced by .001-inch wall silver guide for final operation to minimize the system noise temperature and loss.

D. Construction and Testing of Maser

Rutile crystals

The rutile boules, both doped and undoped, were purchased from the Linde Air Products Company. Chromium doping of 0.1% was originally specified; however, the supplier could only guarantee good single crystal boules of high purity with .04% Cr⁺³ or less. The boules supplied were maximum purity and .04% Cr⁺³ by weight.

The crystal symmetry axes were found by x-ray analysis and marked on the boule before shipment. This facilitated the machining of the rectangular pieces which were to fill the waveguide.

The waveguide dimensions finally arrived at were $a = 0.030$ inch (0.711 mm), $b = 0.012$ inch (0.305 mm) and a total length of dielectric filled guide of 1.5 inches. Inches will be used when referring to the reduced size waveguide dimensions. Since extensive work was done by machinists who work exclusively in the British system the dimensions were adjusted to be round numbers in inches for their convenience.

The machining of the rutile pieces was done by Insaco, Incorporated in Quakertown, Pennsylvania, to a tolerance of ± 0.0001 inch.

The finished pieces were checked for axis orientation at The Pennsylvania State University Mineral Sciences Laboratory by x-ray diffraction methods. Unfortunately, the first machined crystals were oriented incorrectly and a second set had to be made. These latter crystals were oriented to within one degree of the specifications. The final adjustment of the angles between the magnetic field and the crystal axes is made by means of moving the magnet slightly on its gymbals.

The precession Laue x-rays used for checking axis orientation indicated that the rutile was indeed quite pure and probably a single crystal.

Reduced size waveguide

The reduced size waveguides used for all the various test pieces and the final maser were made by machining a rectangular slot in a brass block about 0.0005 inch larger than the crystal dimensions and then screwing a brass cover over the slot. The interface between the block and the cover was carefully lapped to insure a tight fit. Minimum loss occurred when the cover pressed slightly on the broad dimension of the crystal when tightened down.

Various methods for constructing the waveguide were tried but the above method was the most straightforward and gave the best results.

Some reduction in ohmic loss could be obtained by gold or silver plating the brass waveguide.

Tapered transitions

The tapered transitions into the reduced size, dielectric filled waveguide were designed from the following analysis.

Consider a waveguide of dimensions a and b , partially filled with a dielectric constant ϵ and a width d . The wave impedance for the $TE_{2,0}$ mode in the filled and unfilled portions of the guide are given by Marcuvitz⁽³⁰⁾ as

$$\frac{Z_o(\text{die})}{Z_o(\text{air})} = \frac{1 - \lambda_o/\lambda_g}{\epsilon - \lambda_o/\lambda_g} = \tan \left| \frac{\pi}{\lambda_o} (a - d) \right| \cot \left(\frac{\pi d}{\lambda_d} \right) \quad (76)$$

where

λ_o is the free space wavelength

λ_g is the guide wavelength

$$\lambda_d = \lambda_o/\sqrt{\epsilon}.$$

As before, we look for the waveguide dimensions such that the $TE_{2,0}$ mode is just at cutoff. Cutoff is defined as the point where $\lambda_g \rightarrow \infty$. Thus, we can let $\lambda_g \rightarrow \infty$ in equation (76) and solve for a . The cutoff condition for the $TE_{2,0}$ mode in a partially filled guide is then

$$a = d + \frac{\lambda_o}{\pi} \text{Arctan} \left| - \frac{1}{\sqrt{\epsilon}} \tan \left(\sqrt{\epsilon} \frac{\pi}{\lambda} \right) \right|. \quad (77)$$

Figure 9 shows the result of this equation. The diagram is looking down on the broad dimension of the waveguide which has a height the same as the dielectric filled guide; that is, 0.012 inch. Since the tapered crystal dimensions are fixed, a value for the waveguide width, a , was calculated where the $TE_{2,0}$ mode cut off for points along the length of the tapered crystal. This is shown by the dotted line in Figure 9. The actual waveguide dimensions should be just inside this line and match the RG-(96)/U dimensions on the left and the fully filled guide dimensions on the right. The waveguide is indicated by a solid line in Figure 9. At the end of the tapered crystal the guide is full width but of reduced height. It is then tapered in the b dimension to full height in approximately four wavelengths.

Testing of a transition made to these dimensions gave a VSWR due to the taper to the reduced height guide of < 1.05 and a total VSWR of 1.4 for the complete transition. A VSWR of 1.4 causes about 3% of the power to be reflected. However, by using conventional matching techniques such as a slide screw tuner the mismatch can be reduced to have a VSWR ≈ 1.1 which produces a negligible loss.

Rutile dielectric constant

After the tapered transitions were constructed, a test piece of dielectric filled waveguide had a low input VSWR but was lossy to the point where almost no detectable signal could be transmitted through it. It was felt that the high loss was due either to the rutile having a high loss tangent or to mechanical imperfections in the waveguide.

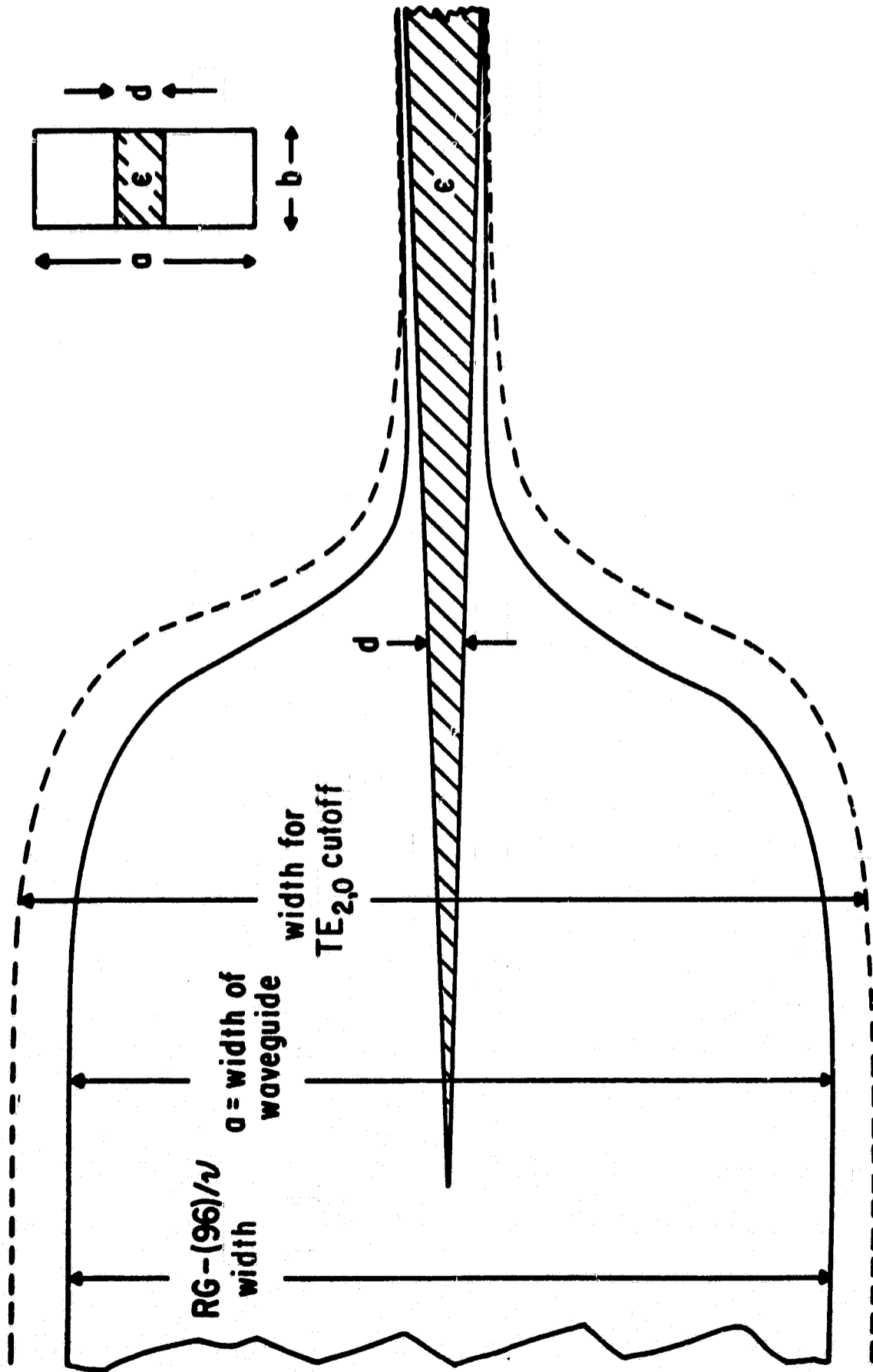


Figure 9 - Tapered Transition

The published loss tangent of rutile is approximately 10^{-3} and should contribute negligible loss even in the fully filled guide. Placing pieces of rutile in high field regions of the full sized waveguide produced only very small losses and these could be accounted for by reflections and the generation of higher order modes. Thus, a high loss tangent was ruled out.

Effort was concentrated on obtaining a good fit of the crystals in the waveguide and a good surface finish on both the waveguide and the crystals. A single 0.5 inch straight section was extensively tested. The net result of constantly improving the fit and finish was that the loss constantly increased, ultimately reaching nearly 40 db.

At this time it was decided that the loss was not due to mechanical imperfections but to a fundamental propagation problem. Cutoff of the dominant $TE_{1,0}$ mode is dependent only on the broad dimension of the waveguide which must be greater than $0.5 \lambda_g$. The full width waveguide, with the crystals lying down the center of the guide, showed only a small loss even if the height of the guide was reduced to that of the crystals. Clearly, the high attenuation must occur somewhere between full width and the fully reduced width. An experiment was then performed to determine the attenuation as a function of waveguide width with the crystals in place. Loss in a 0.5 inch length of waveguide was measured as a function of the width of the air gap on each side of the crystal. The height of the waveguide was the same as the crystal height. The results of this experiment are shown in Figure 10. The attenuation increases rapidly as the width is decreased.

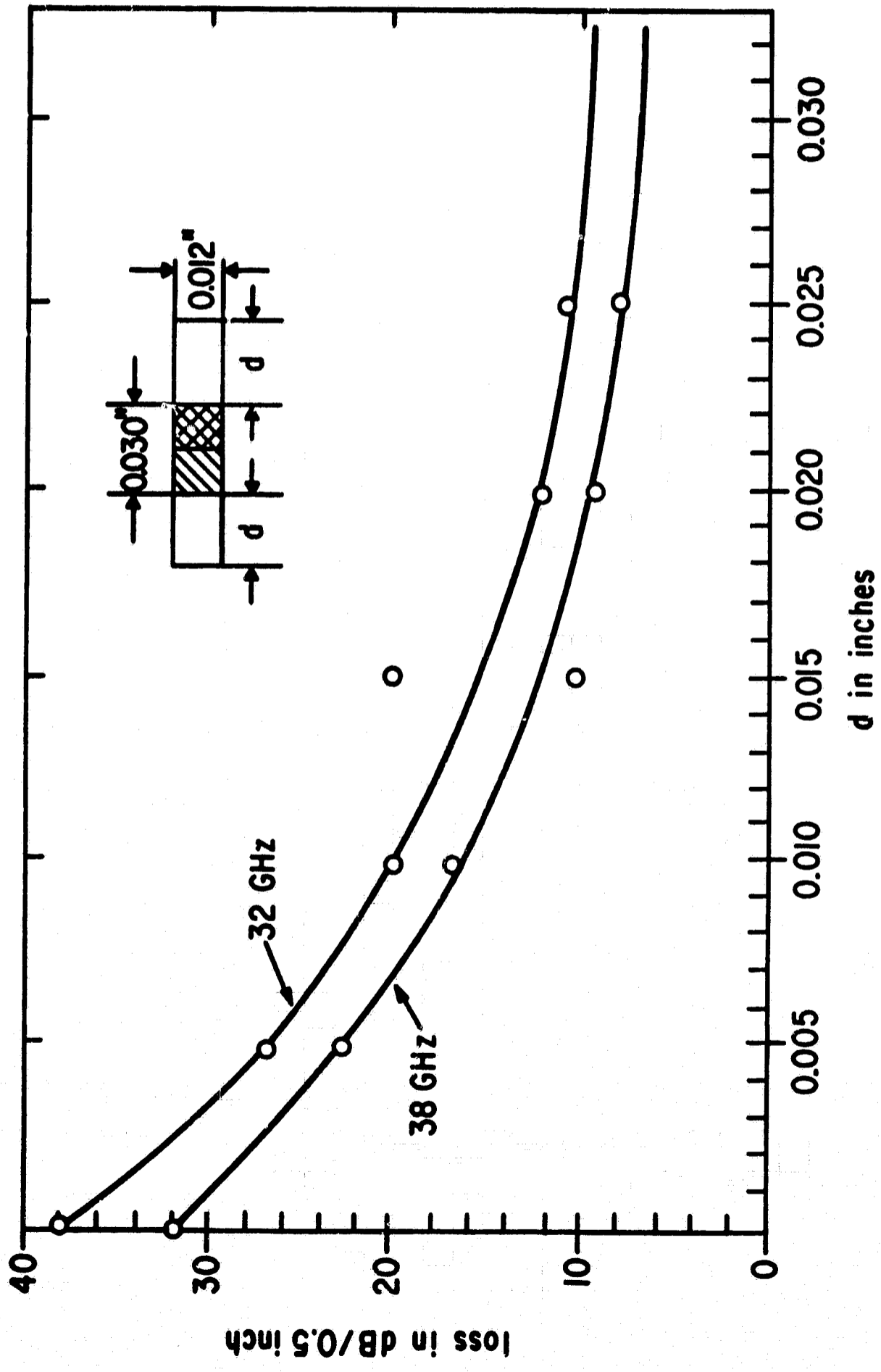


Figure 10 - Attenuation in Partially Filled Waveguide

Also the lower frequency loss increases first, exactly as would be expected as cutoff is approached. In all cases the attenuation was > 40 db with the crystals removed from the waveguide.

The only reasonable explanation for this apparent cutoff is that the dielectric constant of rutile is significantly lower at millimeter wavelengths than reported at the lower microwave frequencies.

A search of the literature indicated that no direct measurement of the dielectric constant of rutile had been made at frequencies higher than 22 GHz and only one measurement was published for a frequency greater than 10 GHz. Consequently, a program to determine ϵ at 36 GHz both at room temperature and at some reduced temperature was initiated.

Measurement of dielectric constant

The method is to set up a transmitter and a length of waveguide containing a traveling probe. The transmission line is terminated in a short with the traveling probe or slotted line a short distance from the short. A null is found in the standing wave pattern set up between the transmitter and short by means of the slotted line. The dielectric sample is then placed in the waveguide next to the short and, since the guide wavelength decreases in the dielectric, the null in the standing wave pattern will be shifted. The complete method is outlined by Redheffer⁽³¹⁾ who gives the following equations for low loss dielectrics:

$$\frac{\text{Tan } (2\pi V)}{V} = \frac{\lambda_g}{d} \text{Tan } (2\pi u) \quad (78)$$

where $V = \frac{d \sqrt{\epsilon - P}}{\lambda}$, $u = \frac{\Delta + d}{\lambda_g}$

and $P = (\lambda / \lambda_c)^2$

d is the length of the dielectric

Δ is the shift in the null position

λ is the free space wavelength

λ_g is the air filled waveguide wavelength

ϵ is the relative dielectric constant.

The loss tangent can be found from

$$\text{Tan } \delta = W \left(\frac{\epsilon - P}{\epsilon} \right) \frac{4\pi \text{Csc } 4\pi u}{4\pi V \text{Csc } (4V) - 1} \quad (79)$$

where $W = \frac{1}{\pi} \frac{1 - R}{1 + R}$.

R is the reflection coefficient and is related to the standing wave ratio σ by

$$\sigma = \frac{1 + R}{1 - R}$$

What is actually measured to determine both the loss tangent and dielectric constant is the null shift Δ , the standing wave ratio σ and the guide wavelength λ_g . Equation (78) is a transcendental equation in ϵ and may be solved by an iterative method. Once ϵ is known, equation (79) can be solved for the loss tangent.

Since a large number of measurements were made from 28 to 39 GHz, a computer solution to equations (78) and (79) was used.

The rutile samples measured were the same rectangular crystals used in the maser. A crystal was placed across the broad dimension of the waveguide which was tapered in height to be the same height as the crystal. The crystal was directly in contact with the shorted end of the guide. The reduced height waveguide presents no problem because in the dominant mode the height of the guide does not affect the propagation parameters as long as it is less than $\lambda_g/2$. One possible source of error is higher order modes being able to propagate in the dielectric material since the guide is the same width as when air filled. However, the effect of higher order modes is just to change the guide wavelength. Their values must fall between the free space wavelength and the dominant mode wavelength. There is also reason to believe that good mode purity existed since the standing wave nulls remained extremely sharp.

The experimental setup for measuring the dielectric constant is shown in Figure 11.

The dielectric constant and loss tangent were measured at both room temperature and at liquid nitrogen temperature (77°K) for two orientations of the crystal.

The dielectric constant was also measured at 1 MHz by the Materials Research Laboratory at The Pennsylvania State University. The method used was to place a wafer of rutile between the plates of a capacitor and measure the change in capacitance.

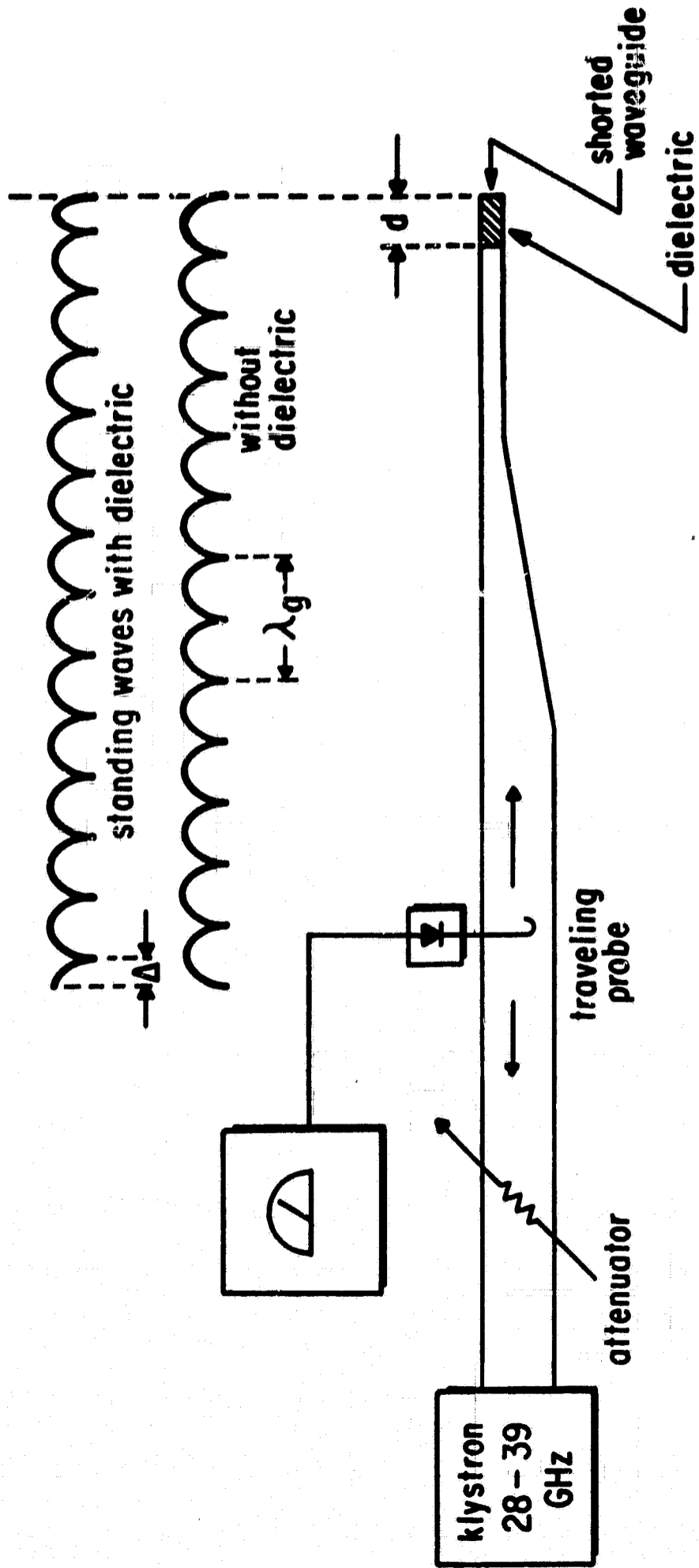


Figure 11 - Method of Measuring Dielectric Constant

The results of the room temperature measurements are shown in Figure 12 and Table 1. Measurements at 77°K were less accurate due to the difficulty in keeping liquid nitrogen, frozen water vapor, and air out of the waveguide. The low temperature dielectric constant at 36 GHz, 90° from the c-axis and 54° from the c-axis, were both near 50 with a $\pm 10\%$ accuracy on the latter number. The 1 MHz result at room temperature is 160 at 54° from the c-axis. The latter is in agreement with the published values. At 77°K $\tan \delta$ was less than .003 at all frequencies.

The results of previous determinations of the dielectric constant are also summarized in Table 1.

The low value of ϵ and the strong frequency dependence at millimeter wavelengths has not been reported previously.

T	f (GHz)	$\epsilon(\theta = 0)$	$\epsilon(\theta = 90^\circ)$	observer
300°K	0.1	170	85	Sabisky and Gerritsen ³²
	10	145	75	Sabisky and Gerritsen
	21	170	87	Sabisky and Gerritsen
	28	-	70	Swanson
	31	-	50	Swanson
	35	60*	40	Swanson
	37	50*	35	Swanson
77°K	0.1	233	120	Sabisky and Gerritsen
	35	50* ± 10	50 ± 5	Swanson
4.2°K	0.1	255	155	Sabisky and Gerritsen

* $\theta = 54.7^\circ$, ϵ should be about 20% higher at $\theta = 0$

Table 1. Dielectric Constant of Rutile

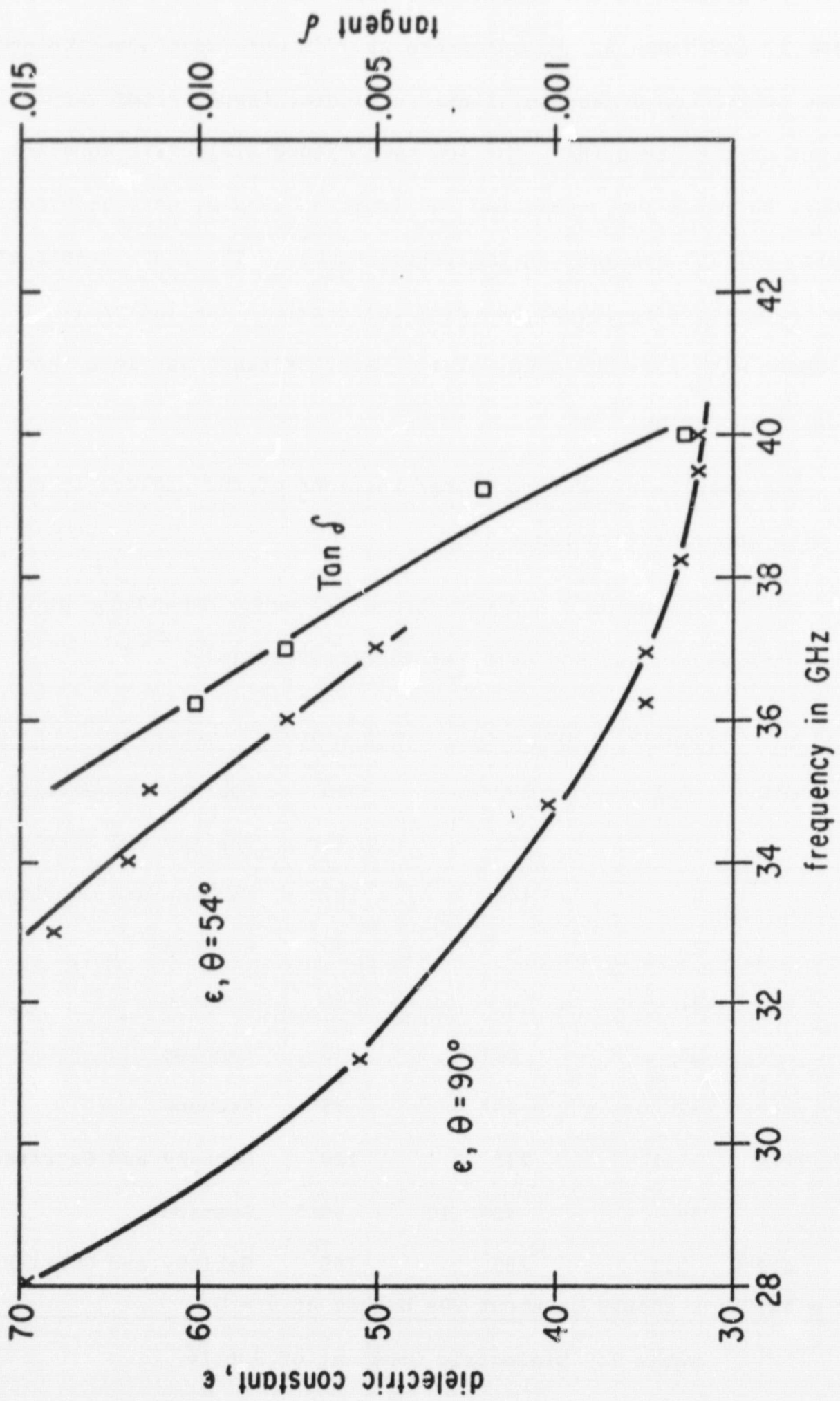


Figure 12- ϵ and $\text{Tan } \delta$ for Rutile at 300°K

Prototype maser

The proper cross section of the fully dielectric filled waveguide based on the revised value of the dielectric constant at 36 GHz is 0.044 x 0.016 inch as compared to the previous size of 0.030 x 0.012 inch. The long rectangular crystals were originally cut to a dimension of 0.015 x 0.012 x 0.5 inch so that one doped and one pure crystal, lying side by side, would fill the proper size waveguide. Three of these crystals, side by side, would give a guide cross section of 0.045 x 0.012 inch. Since the guide height does not contribute to cutoff of the dominant mode it was decided for test purposes to use three of the original crystals as providing nearly the correct waveguide dimensions. Unfortunately, the bends and tapered transition pieces could not be used. At this time a complete new set of crystals was ordered, machined to the proper dimensions.

A prototype maser was constructed using three 0.5 inch long crystals. Two of the crystals were doped and one undoped. This device is shown in Figure 13. The input waveguide first makes a 90° E-plane bend, tapers to a height of 0.012 inch, makes two 90°, H-plane resonant bends in the reduced height guide and then tapers abruptly into the fully filled waveguide.

The total loss at room temperature was 4.8 db with an input VSWR of 1.8. The specific contributions to the total loss are as follows:



Figure 13 - Prototype Maser

brass waveguide including bends	2.0 db
reflections at input and output	0.8 db
rutile filled waveguide	<u>2.0 db</u>
	4.8 db

The loss decreased to approximately 3.8 db at liquid helium temperature. The total loss at the 90 GHz pump frequency was 2.7 db.

Resonance absorption at 36 GHz was immediately observed at the predicted fields of 1.7, 8.6, and 15.1 kgauss. The absorption in the resonance lines was approximately 1.5 db at a -42 dbm input. The two doped crystals were apparently slightly misaligned with each other because the resonance lines were doublets. The separation of the lines indicated a 0.5° misalignment about an axis parallel to the long dimension of the waveguide.

When it was established that the resonance energy levels were correct the pump was turned on. Maser action was observed, using an input signal at 36.0 GHz and sweeping the magnetic field slowly past the point at 15.1 kgauss where the signal transition is 36 GHz. On the initial attempt there was a 1.5 db absorption with the pump klystron off. With the pump klystron on the output signal increased by 2.1 db giving an electronic gain of 3.6 db and a net gain of 2.1 db. Since saturation of the signal transition occurs at high input levels, the gain increases as the input decreases to a point where the signal is "small". The gain continued to increase more or less linearly down to an input level of -55 dbm which was the limit of resolution

of the crystal video detector. At this point, the electronic gain was 7.0 db with a bandwidth of 80-100 MHz.

It should be noted that the gain, as a function of input power, presents no problem in actual operation of the maser since expected signals are on the order of -150 dbm. It is felt that the gain becomes constant near the point of maximum gain observed. However, this cannot be determined until an actual radiometer is used in back of the maser to detect lower level signals.

The electronic gain in the reverse direction was approximately 1.5 db with the amplification just equaling the absorption. In this case no ferrite isolation is needed, although as more gain is achieved it may become necessary to employ additional isolation.

The operation of the prototype maser amplifier is summarized below.

Signal frequency	36.0 GHz
Pump frequency	90.0 GHz
Magnetic Field	15.1 kgauss
$\theta = 54.7, \phi = 45^\circ$	
Paramagnetic absorption	1.5 db
Absorption bandwidth	≈ 200 MHz
Electronic gain	7.0 db/0.5 inch minimum
Net gain	5.5 db/0.5 inch minimum
Bandwidth	80-100 MHz
Net reverse gain	0.

The ohmic losses were reduced to 3.1 db with about 1.5-2.0 db, representing constant loss at the input and output which is independent of the length of the active portion of the slow wave structure.

The energy levels of the two individual crystals not being coincident probably decreased the gain due to cross relaxation effects. Also, the filling factor was low since only one crystal out of three was actually being used.

This is the first reported maser action in rutile for push-pull pumping, double ion site operation, and high magnetic field region.

Operation with larger cross-section crystals

A new set of rutile crystals was machined for a fully filled waveguide cross section of 0.044 x 0.016 inches. The rectangular crystals were each 0.5 x 0.022 x 0.016 inches so that one Cr^{+3} doped and one pure rutile crystal would fill the guide. At the same time several 180° u-turns with a 0.100 inch inside radius and compatible tapered transitions were machined.

The new crystals were placed in the same device as shown in Figure 13 with the waveguide enlarged to the required dimensions. The minimum insertion loss was 3.0 db, 0.8 lower than the previous smaller waveguide. Furthermore, the loss in a 0.5 inch, crystal filled, straight test section, without the series of 90° resonant bends, was 1.4 db minimum.

Maser action was obtained at a 37.17 GHz signal frequency with a magnetic field of 15.3 kgauss and a pump frequency of 92.3 GHz. After carefully adjusting the angles of the magnetic field, the magnitude of the field and the pump frequency, a maximum electronic gain of 20 db and a net gain of 16 db was observed at an input signal level of -40 dbm. The electronic gain increased more or less linearly from 6 db at a -25 dbm input to 20 db at a -40 dbm input. The resonant absorption was near 4 db over this input range giving a net gain of 2 db at a -25 dbm input increasing to 16 db at -40 dbm input. Levels below -40 dbm could not be detected so it is not known whether the electronic gain increased beyond 20 db at still lower input levels.

This extremely high gain for a total active length of 0.5 inch is almost 10 db greater than theoretically predicted. The possibility that the maser was oscillating rather than amplifying was considered. However, the input signal was modulated at 1 KHz and the detector contained an audio stage sharply tuned to 1 KHz, thus the only detectable signals could be amplified input signals. The continuous wave power which would come from oscillations or from the pump could not be detected even at relatively high levels.

The bandwidth of the 3 db points was $100 \text{ MHz} \pm 10 \text{ MHz}$, very slightly wider than the previous result.

Ferrite isolator

In the event that additional reverse isolation would be needed along the maser slow wave structure, experiments were carried out using ferrite material along one side of the fully filled waveguide.

Ferromagnetic resonance absorption is similar to paramagnetic resonance as previously discussed in that the unpaired electron spins in the ferrite precess about an applied magnetic field and can interact with and absorb an r.f. field of the proper frequency and polarization. An additional property of ferrites is that the internal field, H_i , is a function of the magnetization of the ferrite and is related to the external field, H_a , by the Kittel equation,⁽³³⁾

$$H_i = \{ [H_a - (N_z - N_x)M_s] [H_a - (N_z - N_y)M_s] \}^{\frac{1}{2}} \quad (80)$$

where

H_i = internal field

H_a = applied field (in z-direction)

M_s = saturation magnetization

$N_x + N_y + N_z = 4\pi$ = demagnetizing factors.

The frequency at which resonant absorption will occur is

$$\nu = g\beta H_i ,$$

where g is equivalent to the Lande g factor and is a property of the particular ferrite and β is the Bohr magneton equal to 1.4 MHz/gauss.

The demagnetization factors are a function of the shape of the ferrite sample and are, roughly speaking, large if that particular dimension is small. For example a long round needle in the z-direction would have $N_x = N_y = 2\pi$ and $N_z = 0$. A thin disc in the y-z plane would have $N_x = 4\pi$ and $N_y = N_z = 0$. A sphere would have $N_x = N_y = N_z = 4/3\pi$.

The first ferrite tested was a nickel ferrite supplied by Trans-Tech Incorporated.[†] It was designated as T T 2-101 with $4\pi M_s = 3$ kgauss, $g = 2.21$, and an absorption linewidth of 350 oersted. The ferrite was broken into a coarse powder, mixed with a small amount of acrylic lacquer and painted on the narrow side of the 0.5 inch long undoped crystal next to the waveguide wall. At a signal frequency of 36.0 GHz there was 7 db of resonance absorption in the forward direction and less than 1 db in the reverse direction. Absorption occurred at a magnetic field strength of 11.25 kgauss with an exceptionally large linewidth of 4 kgauss at the 3 db points. If it is assumed that in the powdered ferrite all the demagnetizing factors are equal then the Kittel equation becomes simply

$$\nu = g\beta H_a . \quad (81)$$

[†]Trans-Tech Incorporated, 12 Meen Avenue, Gaithersburg, Maryland

This is consistent with the result of resonant absorption at 36.0 GHz, 11.2 kgauss and a g factor of 2.29, only slightly larger than the published value of $g = 2.21$. The large linewidth can be explained by assuming that each individual ferrite chip had a strong shape factor but that the chips, held in place by the lacquer, were oriented in random directions. The internal field in each chip could range from $H_a + 4\pi M_s$ to $H_a - 4\pi M_s$ depending on its shape and orientation. With $4\pi M_s = 3$ kgauss the maximum line width could be ± 3 kgauss or 6 kgauss centered about H_a which is consistent with a measured 3 db width of 4 kgauss centered about 11.2 kgauss.

This particular isolator, however, was not suitable since at the maser operating frequency of 36 GHz the required magnetic field is 15.1 kgauss whereas the TT 2-101 ferrite absorption peak was at 11.2 kgauss.

Trans-Tech supplied another nickel ferrite sample designated as TT 2-113 with $4\pi M_s = 500$ and a g factor of 1.59. The lower g factor should produce a resonance at 33 GHz with a 15.1 kgauss field. With the broad bandwidth previously observed it was hoped that 36 GHz would be within the resonance linewidth. An isolator was again made using the same technique of powdering the ferrite and painting it on the undoped crystal on the opposite side of the waveguide as the doped crystal.

A resonance absorption of 5 db was observed for a 0.5 inch length at a frequency of 36.4 GHz and a field of 15.1 kgauss. The 3 db line width was 1.8 kgauss. This gives a g factor of 1.72 as opposed to 1.54 as reported by Trans-Tech. The isolator resonance absorption was nearly centered about the 36 GHz operating frequency at the 15.1 kgauss magnetic field required for maser operation. The linewidth is broad enough so that for different frequency maser operation the isolator will track the maser energy levels.

Increased absorption should be easily obtained by increasing the amount of ferrite material. The total amount of ferrite painted on the crystals was probably less than a milligram. It was not determined whether the presence of the ferrite perturbed the Cr^{+3} energy levels as has been the case in some maser applications.

This is a particularly simple way to make a ferrite isolator since the difficult task of machining the ferrite is eliminated. Ferrites are commercially available with g values ranging from 1.5 to 2.7. The large linewidths produced by the powdered ferrite give a fairly wide latitude in choosing g and H_a for resonance at a particular frequency.

E. Final Maser Amplifier

Description

A drawing of the final maser is shown in Figure 14. Two 0.5 inch long straight sections are connected by a 180° turn. The active straight sections have a cross section of 0.016 x 0.045 inch. The input and output tapers are approximately 0.4 inch long and taper into a air-filled guide of 0.280 x 0.016 inch cross section. The reduced height, air filled guide then turns 90° in the E-plane and tapers into the full-sized RG-(96)/U waveguide. The 180° bend and the tapered transitions are filled with pure rutile while the active region of the guide is filled with pure rutile in one half and Cr⁺³ doped rutile in the other.

No ferrite isolation is used.

The waveguide is a slot machined in a brass block with a cover screwed on top of the block. An aluminum foil gasket was used between the block and the cover.

Maser operation

The maser was operated at three widely spaced frequencies representing approximately the tuning range of the maser. Table 2 summarizes the maser operation. The gain is the maximum gain measured for an approximately -50 dbm input signal. As input power is decreased the gain is still increasing at -50 dbm; thus, it is possible that still higher gains may be realized when the maser is mated with a radiometer and lower level signals can be detected.

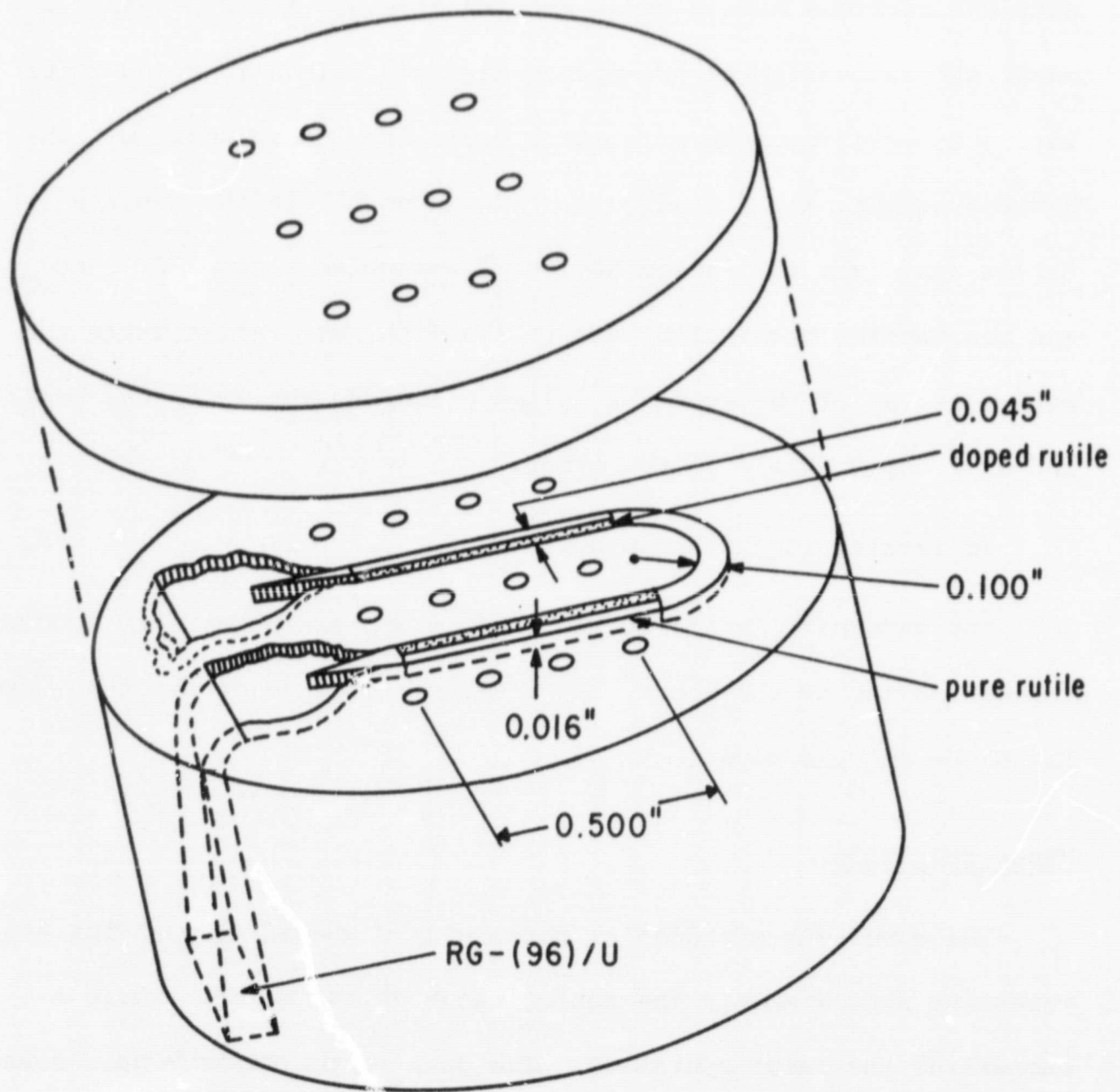


Figure 14 - 36 GHz Maser

The method of measuring gain was to apply a signal to the maser and observe the output voltage of the crystal video receiver. The maser pump was then turned off, deactivating the maser. The input signal was increased to obtain the same output level as when the maser was operating. The increase in signal level is the maser electronic gain. Resonant absorption and ohmic loss can be measured by a simple substitution method with the pump off. These are subtracted from the electronic gain to obtain the actual, usable maser amplifier gain.

Signal frequency	33.81 GHz	36.10 GHz	38.75 GHz
Pump frequency	86.4 GHz	90.2 GHz	96.5 GHz
Magnetic field	14.5 kgauss	15.1 kgauss	15.9 kgauss
Electronic gain	15 db	28.5 db	11 db
Resonance Absorption	5 db	6 db	5 db
Net maser gain	10 db	22.5 db	6 db
Absorption linewidth (3db)	-	400 MHz	400 MHz
Maser Linewidth (3db)	-	170 MHz	150 MHz
Front to back gain ratio	-	5:1	4:1
Operating temperature	4.2°K	4.2°K	4.2°K

Table 2. Maser Operating Parameters

The linewidth was measured by using a constant input frequency, and slowly sweeping the magnetic field past the resonance point. This gives the linewidth in magnetic field units which can be converted to frequency by knowing the dependence of magnetic field on resonant

frequency. For instance, in the vicinity of 15 kgauss the signal transition changes 2.5 GHz/kgauss. Thus, a linewidth of 0.1 kgauss corresponds to 250 MHz.

Gain and bandwidth

The maximum observed net gain at 36 GHz was 22.5 db for a total active length of 1.0 inch. If this is compared with the previous result of 16 db of net gain for a 0.5 inch active length, it appears that the final gain is too low. This can be accounted for by two effects. First, the linewidth for the one inch long maser is 150 MHz as compared to 100 MHz for the one half inch maser. If the two active crystals in the longer maser are not precisely aligned with each other, the resonance lines will also be slightly separated. This amounts to stagger tuning of series amplifiers to increase the bandwidth but which unavoidably decreases the gain. The second effect is that saturation may have had a larger effect in the higher gain maser since in neither case could signals of a low enough level be used to completely eliminate saturation.

The 22.5 db net gain is the gain due to maser action only. In an actual amplifier this is reduced by all ohmic losses present. The total ohmic loss from the input to the output of the cryogenic dewar was 7.0 db. This gives a usable gain of 15.5 db. However, these ohmic losses are not an intrinsic property of the maser and can be reduced to some extent. Waveguide losses make up approximately 3 db and should ultimately be reduced to 1.5 db. The other 4 db is in the maser slow wave structure. Previous loss measurements indicate that

this could be reduced to as low as 2 db by careful machining of the components.

Comparison with theory

The Cr^{+3} energy levels were found to agree well with those given by the secular equation (equation 51), using Gerritsen's values for the constants D and E.

In the case of maser action with only one doped crystal, where there is no stagger tuning, the absorption linewidth was on the order of 200 MHz with a maser linewidth of approximately 100 MHz. This is a larger linewidth than reported previously for chromium doped rutile.⁽³⁴⁾ Some broadening is undoubtedly produced by magnetic field inhomogeneties due to the small solenoid used.

The relation between maser linewidth and absorption linewidth is given by Siegman⁽³⁵⁾ as

$$\Delta\nu = \Delta\nu_L \left[\frac{3}{G_{\text{db}} (\nu_o)^{-3}} \right]^{\frac{1}{2}} \quad (91)$$

where

$\Delta\nu$ is the 3 db maser linewidth

$\Delta\nu_L$ is the 3 db absorption linewidth

G_{db} is the maser gain in db

ν_o is resonance center frequency

For a gain of 15 db, $\Delta\nu/\Delta\nu_L = 0.5$ which is in good agreement with the results.

The gain calculated in equation (68), using $\epsilon = 70$, $\Delta f_L = 200$ MHz, $N = 2 \times 10^{19}/\text{cm}^3$, $\eta = 1/2$, $\sigma = 1$ and I, the inversion ratio, equal to

$v_p/v_s - 1$ is 5.6 db for a 1.0 inch long slow wave structure. The observed net gain was 22.5 db. The difference between the theoretical gain and the actual gain partially depends on the inversion ratio I . In the derivation of the magnetic Q_m (equation 69), Siegman⁽³⁵⁾ states that if the relaxation rates, w_{ij} , are all equal, then the inversion ratio will be given by $v_p/v_s - 1$. However, if the relaxation rates are not all equal, in the optimum case for push pull pumping, the inversion ratio can be as large as $2 v_p/v_s - 1$. In the gain calculation, I could be as large as 4 rather than 1.5 which was used. A value of $I = 4$ gives a gain of 15.0 db, assuming all the other factors in equation (68) are correct. This is still a factor of 1.5 too low. The only other variables in equation (68) which could easily account for this discrepancy are the total number of spins, N , and the slowing factor, S . Which, or if either, of these is in error, is not known at this time.

The low value of the dielectric constant has not been reported previously. The optical frequency dielectric constant is approximately four; thus, the value of ϵ must decrease somewhere between microwave and optical frequencies. However, this relaxation ordinarily takes place slowly, in the infrared region, rather than rapidly in the mm region. The possibility of a resonance effect at millimeter wavelengths exists, but to verify this, measurements of ϵ over a wide range of frequencies, possibly extending to submillimeter wavelengths would have to be made.

IV. SUMMARY

A. Statement of Problem

The large amount of internally generated noise in conventional millimeter wavelength radiometers produces an undesirable signal to noise ratio when observing weak radio sources. The minimum detectable signal of a receiver is directly proportional to the receiver noise. One way of obtaining a major reduction in receiver noise is through the use of a maser preamplifier at the input of the receiving system.

In particular, a maser radiometer operating in the 8 millimeter "atmospheric window" would make weak radio sources available for observation which were previously below the minimum detectable level.

B. Procedure

The procedure followed was to make a theoretical study of a maser radiometer system and to design a practical system making use of previous maser research while considering the intended use in radio astronomy. A prototype maser was constructed to confirm or deny the theory and then a final maser amplifier was constructed using the information obtained from the prototype.

C. Results

A significant fraction of the total effort was spent not on the maser itself but on associated equipment such as microwave hardware, the cryogenic system to cool the maser and a high vacuum system for the vacuum insulation of the cryogenic system.

A major deviation from the original design was caused by a re-evaluation of the dielectric constant of rutile. New crystals had to be machined for a larger cross sectional area.

The four Zeeman energy levels of Cr^{+3} in rutile were as predicted by the theory within experimental accuracy.

An unexpectedly large maser gain was observed in the final prototype which allowed the total length of the finished maser to be reduced. An electronic gain of 28.5 db and a net gain of 22.5 db were obtained with a total active maser length of 1.0 inches. This gain is not completely accounted for by the theory.

Ohmic losses in the waveguide and maser amounted to 7 db giving an overall usable gain of 15.5 db. This is less than the desired value of 20 db, although it is expected that the ohmic loss can be reduced to approximately 3-4 db, giving a final gain of 18 or 19 db.

D. Suggestions for Future Work

The maser amplifier should be connected in front of a conventional radiometer as soon as possible for use as an astronomical instrument.

Further improvements can be made in the maser operation by reducing ohmic losses and possibly by increasing the total active length to increase the maser gain.

The question of the abnormally low dielectric constant of rutile at 36 GHz should be investigated more thoroughly. The effects of frequency, temperature and chromium doping on the dielectric constant and the relationship between the dielectric constant and the loss tangent are specific properties which should be studied.

If the dielectric constant is actually higher than measured, this would increase the slowing factor, S , and increase the calculated gain in the direction of the measured value.

APPENDIX I. Secular Equation Computer Program

```

DIMENSION REAL (4)
10 FORMAT(3F10.3)
20 FORMAT(5X6THETA=,F10.3,5X4HPHI=,F10.3/)
300 FORMAT(5X13HCOMPLEX REAL=,F14.7,5X13HCOMPLEX IMAG=,F14.7/)
600 OFORMAT(10X6HFIELD=,F4.1,3X24HRESONANCE ENERGY IN GC.=,3F9.2,
1 3X4HSIG=,F7.3,3X6HPUMP1=,F7.3,3X6HPUMP2=,F7.3/)
51 READ 10,THETA,PHI,FIELD
IF (FIELD) 66,41.66
66 CONTINUE
PRINT 20,THETA,PHI
THETA=3.1416/180.*THETA
PHI=3.1416/180.*PHI
D=0.550
E=0.270
P=0.01
Q=-6.0
67 H=(1.97*.9273/(.6627*29.98)*FIELD
REAL1=0.0000
REAL2=0.0000
REAL3=0.0000
REAL4=0.0000
AO=1.
A1=0.
A2=-((5./2.)*H*H+2.*D*D+6.*E*E)
OA3=H*H*(2.*D-6.*D*(COS(THETA))**2 -6.*E*(SIN(THETA))**2
1*COS(2.*PHI))
OA4=(1./2.)*H*H*(D*D-6.*D*(COS(THETA))**2 +9.*E*E*COS(2.*THETA)
1+12.*D*E*(SIN(THETA))**2 *COS(2.*PHI))+(9./16.)*H**4
2+(D*D+3.*E*E)**2
100 BO = AO
B1 =A1-P*BO
B2 = A2 - P*B1 - Q*BO
B3=A3-P*B2 - Q*B1
B4 = A4 -P*B3 - Q*B2
CO = BO
C1 =B1 - P*CO
C2 = B2 -P*C1 -Q*CO
C3= C1*C1*Q- C2*(Q*CO-B2)
DELP = (B3*(Q*CO-B2) +C1*(B4+P*B3))/(-C3)
DELQ=(B3*0*C1+C2*(B4+P*B3)) /C3
QUAN1 = ABS( DELP)
IF (QUAN1-1.E-6) 60,70,70
70 P=P + DELP
60 QUAN2=ABS(DELQ)
IF (QUAN2-1.E-6) 74,90,90
90 Q=Q+DELQ
74 SUM = QUAN1 + QUAN2
IF (SUM-2.E-6) 80,100,100

```

```
80 CONTINUE
  A=1.
  B=P
  C=Q
  TERM = (B**2-4.*A*C)
  IF (TERM) 11,21,21
11 CMPXR=-B/(2.*A)
  CMPXI=SQRT(-TERM)/(A*2.)
  PRINT300,CMPXR,CMPXI
  GO TO 31
21 REAL1=(-B+SQRT(TERM))/(2.*A)
  REAL2=(-B-SQRT(TERM))/(2.*A)
31  A=B0
  B= B1
  C=B2
  TERM = (B**2-4.*A*C)
  IF (TERM) 77,78,78
77 COPXR=-B/(2.*A)
  COPXI=SQRT(-TERM)/(A*2.)
  PRINT300,COPXR,COPXI
  GO TO 51
78 REAL3=(-B+SQRT(TERM))/(2.*A)
  REAL4=(-B-SQRT(TERM))/(2.*A)
  REAL(1)=REAL1*29.98
  REAL(2)=REAL2*29.98
  REAL(3)=REAL3*29.98
  REAL(4)=REAL4*29.98
  DO 79 = I=1,4
  K=4-1
  DO 79 J=1,K
  IF(REAL(J)-REAL(J+1)) 79,79,81
81 TEMP=REAL(J)
  REAL(J)=REAL(J+1)
  REAL(J+1)=TEMP
79 CONTINUE
  PUMP1=REAL(4)-REAL(2)
  PUMP2=REAL(3)-REAL(1)
  SIG=REAL(3)-REAL(2)
  RESA=REAL(4)-REAL(3)
  RESB=REAL(2)-REAL(1)
  RESC=REAL(4)-REAL(1)
  PRINT600, FIELD, RESA, RESB, RESC, SIG, PUMP1, PUMP2
  FIELD=FIELD-0.5
  IF(FIELD) 51,51,67
41 STOP
```


APPENDIX II. Rutile Crystal Structure

Figure 15 shows the crystal structure of rutile and the two non-equivalent magnetic complexes at P and P'.

Rutile belongs to the space group D_{4h} , i.e., the crystal has a main four-fold symmetry axis, labeled the c-axis, 2 two-fold symmetry axes perpendicular to the c-axis, labeled a-axes and a reflection plane perpendicular to the c-axis.

The Cr^{+3} and Ti^{+4} ion at P is surrounded by six oxygen ions labeled A through F in Figure 15. The magnetic coordinate system for ion P is labeled x, y, and z. Ion P' is likewise surrounded by six oxygen ions. However, the magnetic coordinate system for ion P', labeled x', y', and z' is rotated 90° about the z-axis from the unprimed coordinate system. Thus, there are two magnetically non-equivalent ion sites.

When viewed in either a-c plane (45° from the y or y' axis), the two ion sites appear as mirror images with identical magnetic properties. Maser operation with the magnetic field in either a-c plane is known as double ion site operation for this reason.

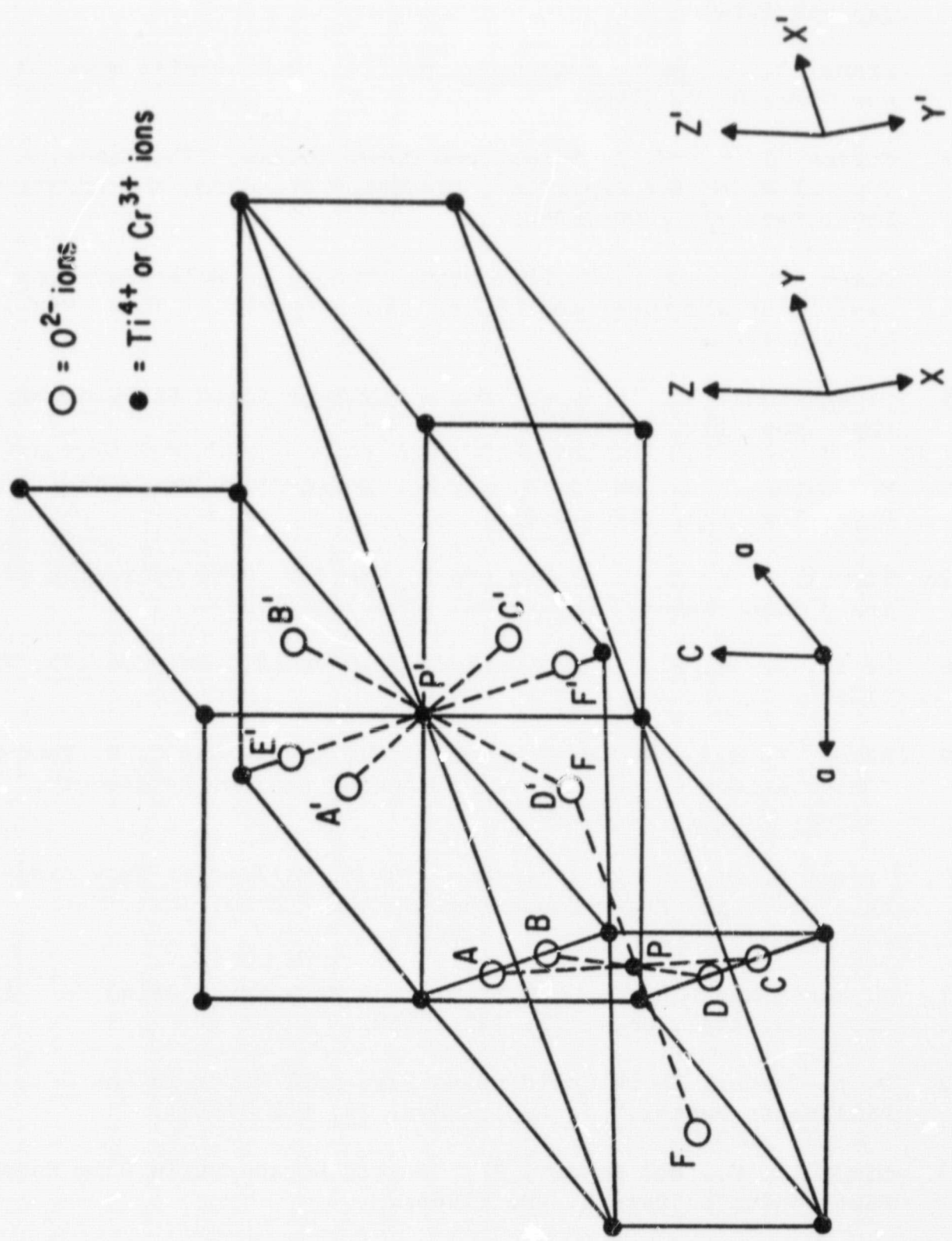


Figure 15 - Crystal Structure of Rutile and Magnetic Axes

BIBLIOGRAPHY

1. Friis, H. T., "Noise Figures of Radio Receivers," Proc. I.R.E. 32, 419 (1944).
2. Kraus, J. D., Radio Astronomy, pp. 241, McGraw-Hill Book Co., New York, N. Y. (1966).
3. Gordon, J. P., H. Z. Zeiger and C. H. Townes, "The Maser, A New Type of Microwave Amplifier, Frequency Standard, and Spectrometer," Phys. Rev. 99, 1264 (1955).
4. Besov, N. G. and A. M. Prokhorov, "Theory of Molecular-Beam Oscillator and Power Amplifier," Zh. Eksperim. i Thor. Fiz., 30, 560 (1956).
5. Bloembergen, H., "Proposal for a New Type Solid State Maser," Phys. Rev. 104, 324 (1956).
6. McWhorter, A. L. and J. W. Meyer, "Solid-State Maser Amplifier," Phys. Rev. 109, 312 (1958).
7. Scovil, H. E. D., G. Feher and H. Scaidel, "The Operation of a Solid State Maser," Phys. Rev. 105, 762 (1957).
8. Price, R., et al., "Radar Echoes from Venus," Science 129, 751 (1959).
9. Alsop, L. E., J. A. Giordmaine, C. H. Mayer, and C. H. Townes, "Observations Using a Maser Radiometer at 3 cm Wavelength," Astron. J. 63, 301 (1958).
10. Arams, F. R., and B. J. Peyton, "Eight-millimeter Traveling-Wave Maser and Maser-Radiometer System," Proc. Inst. Elec. Electronics Engrs., 53, 12 (1965).
11. S. Foner and L. Mama, "CW Millimeter Wave Maser Using Fe^{+3} in TiO_2 ," J. Appl. Phys. 31, 742 (1960).
12. D. L. Carter, "A CW Solid-state Push-pull Maser in the 5 to 6 Millimeter Region," J. Appl. Phys. 32, 541 (1961).
13. Nixon, W. M., and Genner, R., "Ferric Doped-rutile 8 mm Maser," Electronics Letters 2, 406 (1966).
14. Coatpont, P. and A. Robert, "8 mm Traveling-Wave Maser," Electronic Letters 3, 5 (1967).
15. Zagatin, V. I., and G. S. Mizezhnikov, "Ruby Maser Operating in the 8 mm Range," Radio Eng. and Elec. Phys. 3, 501 (1967).

16. Swanson, P. N., and J. P. Hagen, "8 mm Traveling Wave Maser," *Nature* 218, 158 (1968).
17. Powell, J. L., and Crasemann, B., Quantum Mechanics, Addison-Wesley Publishing Co., Reading, Mass., pp. 394-395 (1961).
18. K. H. B. Wilhelmsson, Lectures on the Quantum Theory of Masers, Research Laboratory of Electronics, Chalmers University of Technology, Gothenburg, Sweden (1962).
19. Ref. 17, pp. 381-394.
20. Bowers, K. D., and J. Owen, *Reports Prog. Phys.* XVIII, 304 (1955).
21. Gerritsen, H. J., et al., *Phys. Rev. Letters* 2, 153 (1959).
22. Bloembergen, Ref. 5.
23. Siegman, A. E., Microwave Solid-State Masers, McGraw-Hill Book Co., New York, p. 255 and p. 309 (1964).
24. Siegman, A. E., "Thermal Noise in Microwave Systems," *Microwave Journ.* 4, 93 (1961).
25. Van Voorhis, Microwave Receivers, Radiation Laboratory Series, Boston Technical Publishers, Lexington, Mass., p. 2 (1964).
26. Same as Ref. 21.
27. Sabisky, E. S., and H. J. Gerritsen, *Proc. IRE* 49, 1329 (1961).
28. Moreno, T., Microwave Transmission Design Data, Dover Publications, Inc., New York, p. 132 (1958).
29. Same as Ref. 23, p. 169.
30. Marcovitz, N., Waveguide Handbook, Boston Technical Publishers, Inc., Lexington, Mass. (1950).
31. Redheffer, R. M., Technique of Microwave Measurements, Radiation Laboratory Series, Boston Technical Lithographers, p. 627 (1963).
32. Sabisky, E. S., and H. J. Gerritsen, "Measurements of the Dielectric Constant of Rutile at Microwave Frequencies," *J. Appl. Phys.* 33, 1450 (1962).
33. Kittel, C., "On the Theory of Ferromagnetic Resonance Absorption," *Phys. Rev.* 73, 155 (1948).
34. Same as Ref. 10.
35. Same as Ref. 23, p. 315.
36. Same as Ref. 23, p. 293.